Applied Research Laboratory

(4)

Technical Report

A LASER-INDUCED FLUORESCENCE
TECHNIQUE FOR MEASUREMENT
OF SLOT-INJECTED FLUID CONCENTRATION
PROFILES IN A PLATE TURBULENT BOUNDARY LAYER

by

T.A. Brungart
H.L. Petrie

PENNSTATE

1855

(4)

The Pennsylvania State University
APPLIED RESEARCH LABORATORY
P.O. Box 30
State College, PA 16804

A LASER-INDUCED FLUORESCENCE TECHNIQUE FOR MEASUREMENT OF SLOT-INJECTED FLUID CONCENTRATION PROFILES IN A PLATE TURBULENT BOUNDARY LAYER

by

T.A. Brungart
H.L. Petrie

Technical Report No. TR 90-006
May 1990

Supported by:
David Taylor Research Center

L.R. Hettche, Director
Applied Research Laboratory

REPORT DOCUMENTATION PAGE

Form Approved
OMB No. 0704-0188

1. AGENCY USE ONLY (Leave blank)	2. REPORT DATE	3. REPORT TYPE AND DATES COVERED
	April 1990	

4. TITLE AND SUBTITLE
A Laser-Induced Fluorescence Technique for Measurement of Slot-Injected Fluid Concentration Profiles in a Plate Turbulent Boundary Layer

5. FUNDING NUMBERS

6. AUTHOR(S)

T. A. Brungart, H. L. Petrie

7. PERFORMING ORGANIZATION NAME(S) AND ADDRESS(ES)

Applied Research Laboratory
Penn State University
P. O. Box 30
State College, PA 16804

8. PERFORMING ORGANIZATION REPORT NUMBER

TR-90-006

9. SPONSORING/MONITORING AGENCY NAME(S) AND ADDRESS(ES)

David Taylor Research Center
Department of the Navy
Bethesda, MD 20084

10. SPONSORING/MONITORING AGENCY REPORT NUMBER

11. SUPPLEMENTARY NOTES

12a. DISTRIBUTION/AVAILABILITY STATEMENT

Distribution Statement "A", approved for public release distribution unlimited

12b. DISTRIBUTION CODE

13. ABSTRACT (Maximum 200 words)

A technique for measuring near instantaneous concentration profiles of a fluid injected through a narrow inclined slot at the wall into a high unit Reynolds turbulent boundary layer is discussed. The concentration profiles are determined by measuring the light intensity emitted from a fluorescent dye premixed into the injectant flow as the injectant convects through an excitation laser beam. The fluorescence intensity is quantified by an electronically shuttered single stage microchannel plate image intensifier coupled to a linear photodiode array. This high resolution technique is being used to study the diffusion of injected polymer solutions away from the near wall region in a flat plate turbulent boundary layer where these solutions are effective in reducing drag.

14. SUBJECT TERMS
Reynolds turbulent boundary layer, concentration profile, fluorescent dye

15. NUMBER OF PAGES
105

16. PRICE CODE

17. SECURITY CLASSIFICATION OF REPORT	18. SECURITY CLASSIFICATION OF THIS PAGE	19. SECURITY CLASSIFICATION OF ABSTRACT	20. LIMITATION OF ABSTRACT
UNCLASSIFIED	UNCLASSIFIED	UNCLASSIFIED	UL

ABSTRACT

A technique for measuring near instantaneous concentration profiles of a fluid injected through a narrow inclined slot at the wall into a high unit Reynolds number turbulent boundary layer is discussed. The concentration profiles are determined by measuring the light intensity emitted from a fluorescent dye premixed into the injectant flow as the injectant convects through an excitation laser beam. The fluorescence intensity is quantified by an electronically shuttered single stage microchannel plate image intensifier coupled to a linear photodiode array. This high resolution technique is being used to study the diffusion of injected polymer solutions away from the near wall region in a flat plate turbulent boundary layer where these solutions are effective in reducing drag.

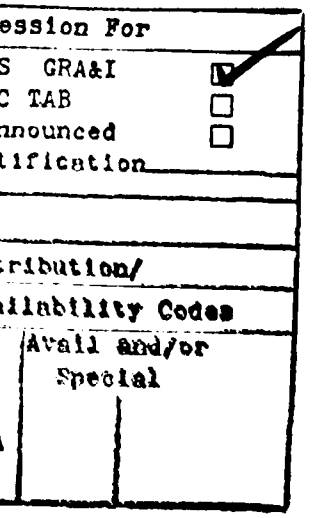

TABLE OF CONTENTS

LIST OF TABLES

LIST OF FIGURES

Figure — Page

Figure | Page

LIST OF SYMBOLS

A - calibration constant (counts/(moles/liter))

a - numerical constant (nondim.)

C - local injectant concentration (moles/liter or wppm)

C' - concentration standard deviation (moles/liter or wppm)

C_A - average local injectant concentration (moles/liter or wppm)

C_f - skin friction coefficient (nondim.)

C_{inj} - injection concentration (moles/liter or wppm)

C_{max} - maximum local injectant concentration (moles/liter or wppm)

D - molecular diffusivity into water (cm^2/s)

G - image intensifier gain (nondim.)

I - laser beam intensity ($watts/m^2$)

I_f - fluorescence intensity ($watts/m^2$)

K - kurtosis (i.e., flatness factor) (nondim.)

i - indicator for a general pixel on the array (nondim.)

j - indicator for a general pixel on the array (nondim.)

k - indicator for a general scan of the array (nondim.)

L - term accounting for lens reflections and imperfections (nondim.)

LDV - Laser Doppler Velocimeter

LIF - Laser Induced Fluorescence

N - noise (counts)

P - term accounting for gate period effects (nondim.)

Q - dye quantum yield (nondim.)

Q_s - flow through area extending from the wall to $Y^+ = 11.6$ in a pure water boundary layer (liters/s)

Re_X - Reynolds number based on distance from boundary layer virtual origin (nondim.)

S - pixel sensitivity (counts/(w/(m^2))

Sk - skewness factor (nondim.)

U - freestream streamwise velocity (m/s)

V - output signal from photodiode array (counts)

W - term accounting for window reflections and imperfections (nondim.)

X - streamwise distance measured from the boundary layer virtual origin or from the injection slot (m) - also denotes streamwise direction

Y - distance measured normal to plate's top surface (m) - also denotes direction normal to plate's surface

Y^+ - distance normal to plate surface in inner variables (nondim.)

Y_0 - location of plate's top surface in the Y-direction

Z - transverse direction normal to the flow

ΔC - polymer concentration bin width (wppm)

ΔX - distance increment in streamwise direction (m)

ΔY - distance increment in direction normal to the plate (m)

δ_{av} - average boundary layer thickness between the slot and X as defined by Poreh and Cermak (1964) (m)

δ_{loc} - local boundary layer thickness (m)

δ^* - boundary layer displacement thickness (m)

ϵ - extinction coefficient (1/(m x moles/liter))

η - Kolmogorov length microscale (m)

θ - boundary layer momentum thickness (m)

λ - diffusion layer thickness (m)

ν - kinematic viscosity (m^2/s)

ρ - density of water (kg/m^3)

τ_w - wall shear stress (Pa)

ACKNOWLEDGEMENTS

I wish to express my appreciation to Dr. H. L. Petrie, Research Associate, for his guidance and technical expertise throughout the course of this investigation. I would also like to thank Mr. W. L. Harbison, Dr. C. L. Merkle, and Mr. S. T. Sommer for their assistance. Finally, I would like to thank the entire staff of the Garfield Thomas Water Tunnel for their assistance and cooperation.

This investigation was conducted at the Garfield Thomas Water Tunnel of the Applied Research Laboratory at The Pennsylvania State University under the sponsorship of the U.S. Navy David Taylor Research Center, Mr. W. G. Souders, technical monitor.

CHAPTER 1

INTRODUCTION

1.1 Background and Objectives

A high-resolution technique for measuring slot injected fluid concentration profiles in a turbulent boundary layer is discussed. This technique, which utilizes laser induced fluorescence (LIF), is capable of measuring concentration profiles in less than 8 microseconds with a spatial resolution normal to the wall exceeding 15 microns. Although the applicability of this LIF technique to a wide variety of injectants is without question, it was developed specifically to study the diffusion of drag reducing polymer solutions in a flat plate turbulent boundary layer. In order to compare the mixing of the polymer to that of a passive scalar, dyed water injection was also studied. Therefore, discussion of injectants will be limited to polymer and water.

The addition of solutions of long-chain polymer to turbulent shear layers is one of the most effective turbulent drag reduction techniques known. Friction reductions in excess of 55% have been reported on flat plates with injection of dilute polymer solutions [Wu and Tulin 1972]. For these studies, the polymer has typically been injected into the turbulent boundary layer through an inclined, narrow slot near the leading edge of the plate.

It is generally accepted that polymeric drag reduction is a result of modifications to the boundary layer buffer region [Lumley 1973, 1977]. More specifically, experiments have shown a suppression of the very small eddies at the high frequency dissipation end of the energy spectrum [White and Hemmings (1976)] and a resistance to vortex stretching [Gadd (1968), Lacey (1974), Falco and Wiggert (1979)]. However, in order to be effective, the polymer must reside in the near wall region where the smallest high frequency eddies occur. The turbulent diffusion of the polymer away from the wall after injection diminishes the concentration near the wall; and, therefore, the local drag reduction levels with increasing streamwise distance.

The objective of this thesis is to discuss in detail a technique for measuring near instantaneous concentration profiles of a fluid injected at the wall into a high unit Reynolds number turbulent boundary layer and to present representative polymer and dyed water results. The concentration profiles are determined by measuring the light intensity emitted from a fluorescent dye premixed into the injectant flow as the injectant convects through an excitation laser beam. The intensity of the emitted fluorescent radiation is quantified by an electronically shuttered single stage microchannel plate image intensifier coupled to a linear photodiode array. The high Reynolds numbers of the subject flows insures that diffusion occurs predominantly by turbulent mechanisms. Therefore,

it may be assumed that the dye and injectant mix as one and their relative concentrations remain constant after injection. The actual injectant concentration may be determined directly by measuring the dye concentration since the ratio of injectant concentration to dye concentration is known.

A few of the many analyses which may be performed on the near instantaneous data include the computation of mean concentration profiles, profiles of higher order central moments, and probability density functions as a function of distance from the wall. The LIF technique is a very powerful, nonintrusive tool capable of achieving a temporal and spatial resolution not possible by previous, more conventional techniques.

1.2 Previous Work

Since the pioneering work of Toms (1949), hundreds of experiments have been conducted to study the effects of polymer additives on turbulent shear flows. A number of investigators have studied the diffusion of wall injected polymer in external boundary layers. Wetzel and Ripken (1970) measured mean concentration profiles of a polymer solution injected at the wall in an open channel flow. Their approach was to draw off samples through small total head probes at various locations in the turbulent boundary layer (TBL). Latto and El Riedy (1976) used similar probe techniques to study diffusion in a flat plate TBL downstream of a

slot injector. Fruman and Tulin (1976) studied how diffusion reduces the polymer concentration at the wall in a flat plate TBL by drawing off samples through narrow slits in the surface. Vdovin and Smol'yakov (1978, 1981) studied the diffusion of polymer in the TBL on the flat wall of a water channel downstream of a narrow injection slot. Again, microsampling tubes were used to measure the polymer concentration profiles.

The conventional probe sampling techniques mentioned above are limited to determining the mean concentration at the probe. Additionally, these techniques are limited in resolution and in the approach to the wall due to the size of the sampling probe relative to the diffusion layer scales within the TBL.

Tiederman et al. (1987) made nonintrusive mean concentration measurements in a low speed rectangular channel with slot injection of polymer. The mean concentration at a given height above the wall was determined by measuring the attenuation of a laser beam due to absorption from a fluorescent dye premixed into the polymer. The beam was directed spanwise across the flow and parallel to the surface. Interestingly, the spanwise average was not steady and had to be temporally averaged. Spatial resolution in the direction normal to the wall was limited to the maximum laser beam diameter across the span of the polymer laden flow which was 500 microns in this case. In the present work, the viscous scales at the wall are 5 to 25 times smaller than in this channel flow, and a higher

resolution technique is required.

Koochesfahani and Dimotakis (1985) studied free shear layer mixing by an LIF technique. The approach taken was to direct a focused laser beam across the mixing layer normal to the approach flow with one of the flows seeded with a fluorescent dye. The local dye concentration of the fluid convecting through the excitation laser beam was determined by measuring the local fluorescence intensity with a linear photodiode array.

The approach taken by Koochesfahani and Dimotakis (1985) has been adopted for the current study with modifications for the higher velocities and smaller spatial scales in the TBL flows of interest. In addition to a photodiode array, the use of a long range microscope and electronically shuttered single stage microchannel plate image intensifier increased the spatial and temporal resolution by factors greater than 6 and 1000, respectively, over that achieved by Koochesfahani and Dimotakis (1985).

CHAPTER 2

EXPERIMENTAL APPARATUS

2.1 Experimental Facility

The current study was conducted in a water tunnel facility at the Applied Research Laboratory of The Pennsylvania State University. The tunnel is a closed circuit, closed jet system with a volume of 15,400 liters and can be operated at velocities up to 24m/sec with pressures from 20 to 414kPa. Free stream turbulence is minimized by a 152mm section of honeycomb with a 25mm core size and a 9:1 contraction section. The cylindrical test section's dimensions are 0.3048m in diameter by 0.76m long. Optical access from each side and below the test section is provided by flat acrylic windows which blend smoothly into the circular walls. A tent with walls of opaque plastic was erected over the tunnel and surrounding work area to prevent extraneous light from entering. A schematic of the tunnel is shown in Figure 2.1.

2.2 Experimental Set-Up: The Flat Plate Assembly

A flat, brass plate 1.2m long and 19.05mm thick was mounted on the horizontal centerplane of the Applied Research Laboratory's 0.3048m diameter test section water tunnel. The plate was constructed with a 2-D adaptation of a Schiebe headform nose for a leading edge and a pitched asymmetric tail in order to achieve both

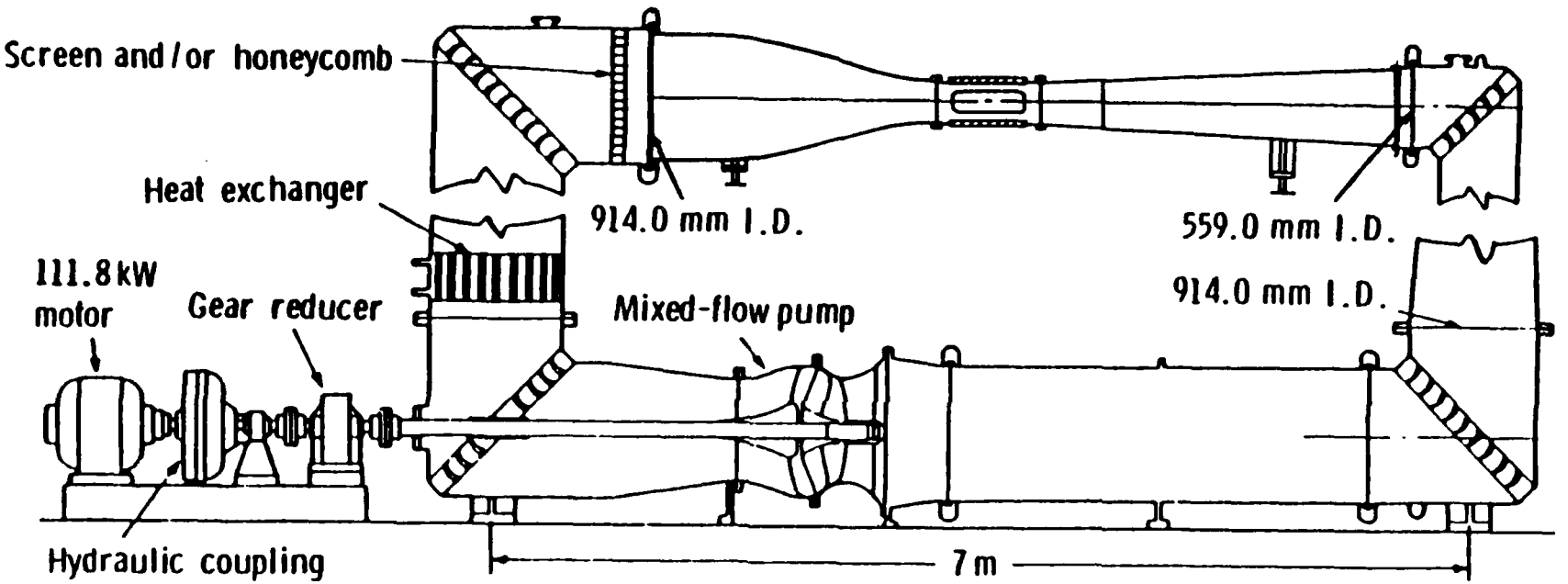

Figure 2.1. Schematic of the Applied Research Laboratory's 0.3048m Diameter Test Section Water Tunnel

good cavitation performance and the proper angle of attack for zero pressure gradient flow over the top surface. The central portion of the plate itself is an acrylic window which provides optical access through the plate from 0.005m to 0.46m downstream of the injection slot. Figure 2.2 is a scale drawing of the plate mounted in the water tunnel test section.

The stainless steel injection slot is located 0.292m from the plate leading edge, has a span of 0.191m, and an exit width of 1.02mm. Two convergent walls form the slot and are at angles of 20 and 30 degrees with respect to the downstream horizontal surface of the plate. A schematic of the injection slot is shown in Figure 2.3.

A small plenum beneath the injection slot is fed by a line from each side of the tunnel. The plenum is packed with a course non-metallic steel wool type material to provide a uniform exit flow of polymer. The polymer is pumped from a storage container to the plenum with a calibrated Masterflex model 7549-56 peristaltic pump manufactured by Cole Parmer Instruments. An air bubble in the supply line plumbing with an approximate volume of 2 to 3 liters effectively removes pump pulsations from the injectant flow. This was verified by visual inspection and from surface mounted flush hot-film anemometer results taken at various stations beginning 12.7mm downstream of the injection slot.

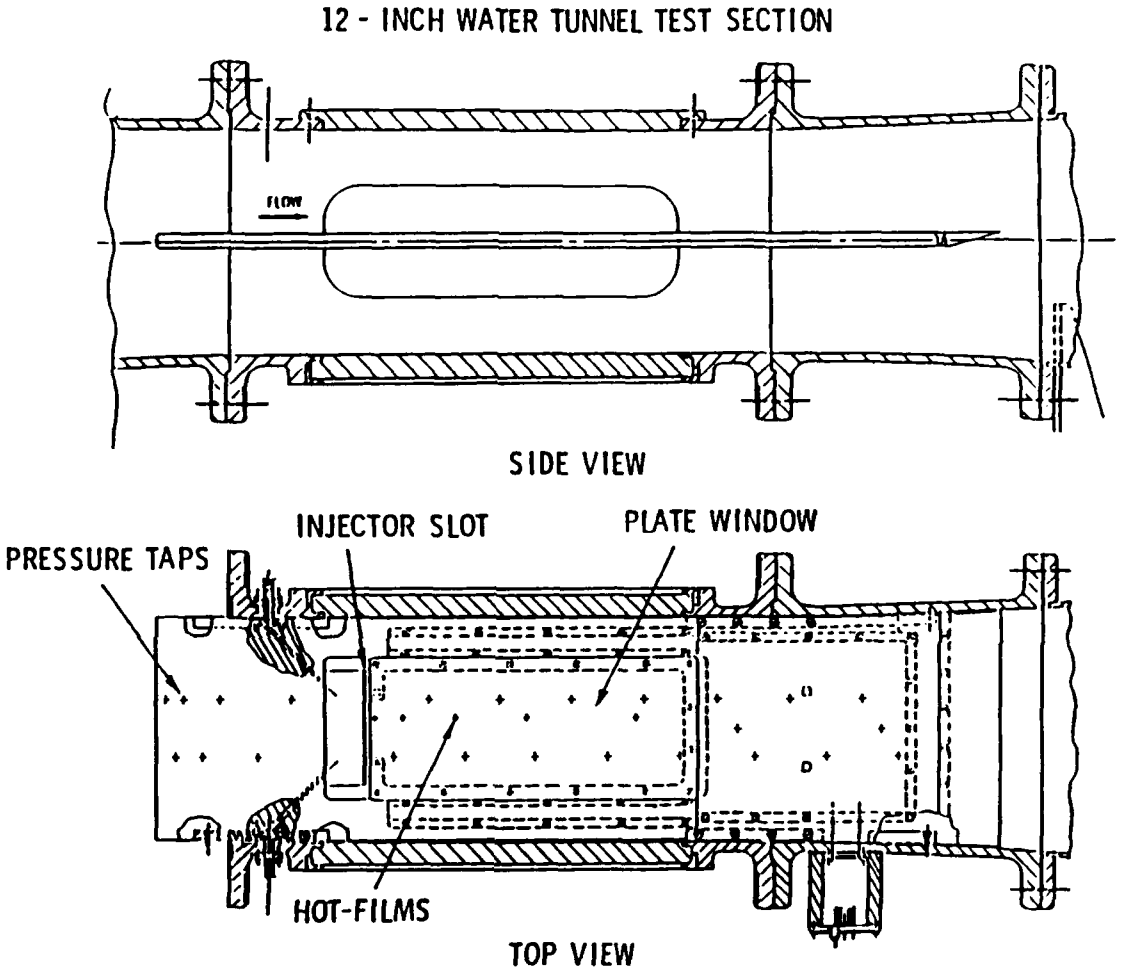

Figure 2.2. Scale Drawing of the Plate Mounted in the 0.3048m Diameter Test Section Water Tunnel

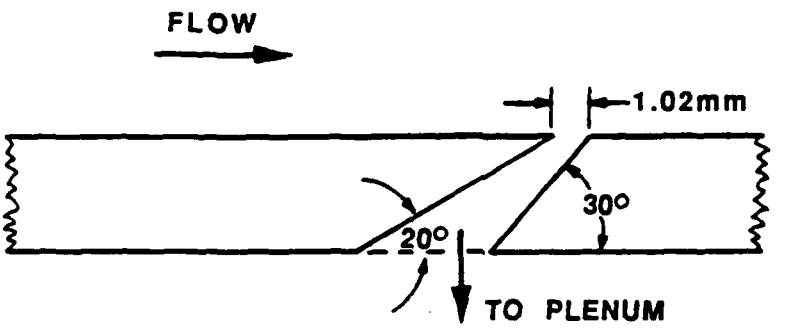

Figure 2.3. Schematic of the Injection Slot

2.3 Flow Characterization

Pressure surveys were taken along the top surface of the plate at 4.6, 9.1, and 13.7m/s, and boundary layer velocity surveys were measured with a one-component Laser Doppler Velocimeter (LDV) system at three streamwise locations at 4.6 and 9.1m/s. The surveys confirmed that a fully developed turbulent boundary layer subject to a near zero pressure gradient exists on the top surface of the test plate. The virtual origin of the boundary layer was 353mm upstream of the injection slot. Table 2.1 compares the measured boundary layer parameters to the values computed from classical empirical relationships for a flat plate. The wall shear stresses and corresponding skin friction coefficients were determined from the velocity profiles via Clauser plots. All the measured values are in excellent agreement with the computed values.

Table 2.1 Comparison of the Measured Boundary Layer Parameters to the Values Computed From Classical Empirical Relationships for a Flat Plate

Location[a] (mm)	U (m/s)	δ_{loc} (mm)	δ_{loc} (C=.14)[b]	δ^* (mm)	δ^* (C=.018)[b]	θ (mm)	θ (C=.014)[b]	C_f	C_f[c]	τ_w (Pa)	τ_w[d] (Pa)
380.27	4.622	5.44	6.71	0.881	0.863	0.642	0.681	0.0030	0.0033	31.91	35.59
	9.153	4.79	6.10	0.738	0.784	0.551	0.618	0.0031	0.0030	127.99	124.57
550.13	4.576	8.46	9.25	1.203	1.190	0.895	0.939	0.0029	0.0031	30.25	32.83
	9.089	6.58	8.38	0.971	1.077	0.738	0.850	0.0028	0.0028	116.14	111.93
753.33	4.567	10.66	12.11	1.447	1.557	1.103	1.229	0.0028	0.0030	29.59	31.07
	9.048	10.56	10.97	1.228	1.411	1.002	1.113	0.0027	0.0027	111.29	109.49

[a] streamwise distance measured from virtual origin

[b] $\delta_{99}, \delta^*, \theta = \dfrac{C \upsilon Re_x^{6/7}}{U}$

δ_{99} : C = 0.14

δ^* : C = 0.018

θ : C = 0.014

[c] $C_f = .026\, Re_x^{-1/7}$

[d] $\tau_w = 1/2\, \rho\, U^2 \dfrac{0.455}{\ln^2[0.06\, Re_x]}$

CHAPTER 3

LASER-INDUCED FLUORESCENCE INSTRUMENTATION

3.1 LIF Excitation Optics

A diagram of the LIF excitation optics used to make the concentration profile measurements is shown in Figure 3.1. The excitation laser and optics are mounted onto a breadboard and supporting frame below the tunnel test section with the supporting frame isolated from the tunnel to minimize vibration. A 5 watt Spectra Physics argon ion laser provides the excitation beam at a 488nm wavelength. The beam is expanded with a 5x beam expander, focused by a 900mm focal length lens, and reflected upward through the bottom window in the tunnel to position the "waist" of the beam at or slightly above the top surface of the plate. The laser beam passes through the plate perpendicular to its surface. The combination 5x beam expander and 900mm focal length lens produce a beam waist to the e^{-2} intensity level of approximately 90 microns. The excitation laser is operated in a constant power mode that limits output power variations to less than 0.5%. The excitation laser power used is 350mW.

3.2 LIF Imaging Optics, Electro Optics, and Electronics

A diagram of the LIF imaging optics, electro optics, and electronics used to make the concentration profile measurements is

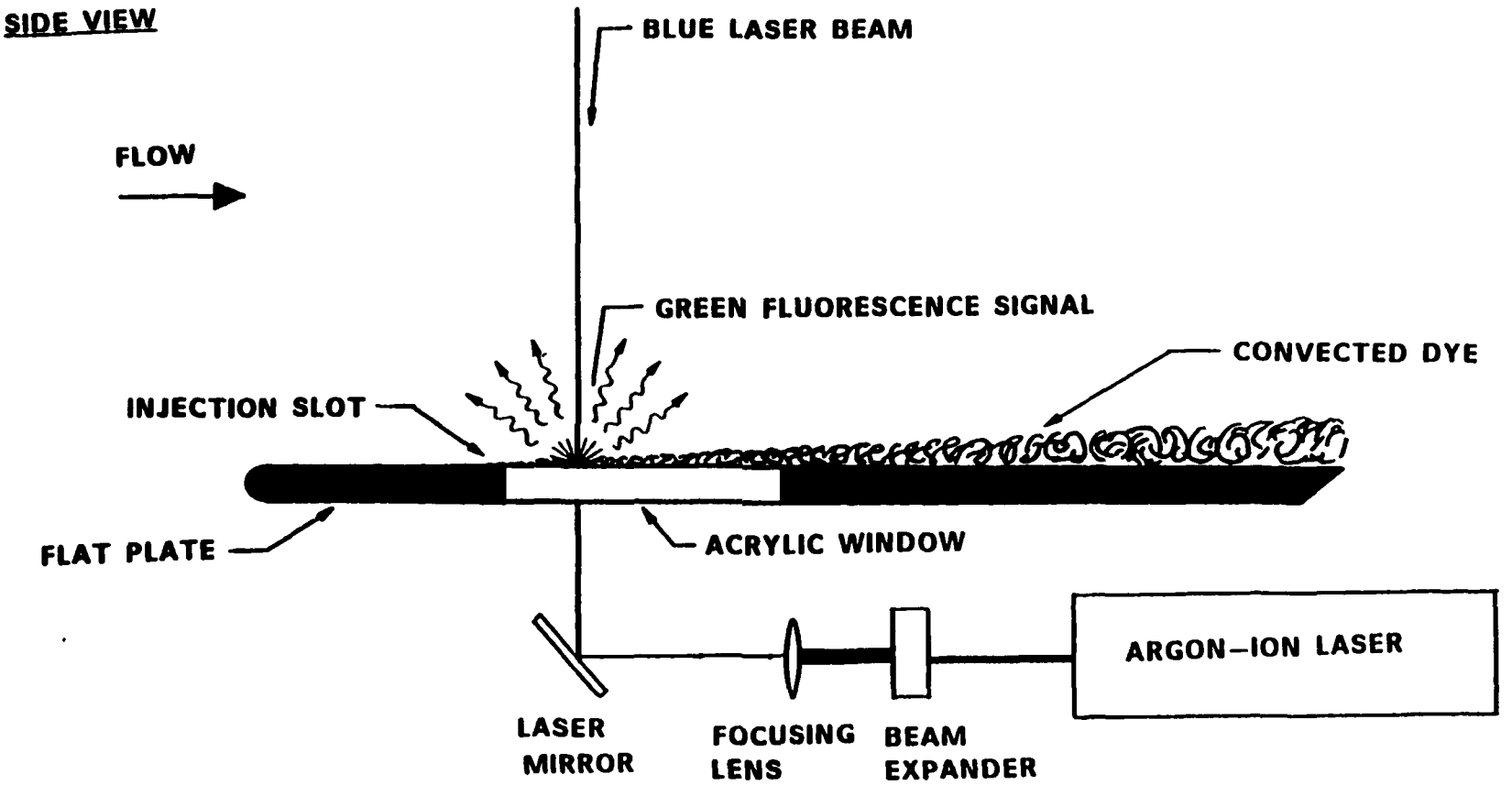

Figure 3.1. LIF Excitation Optics

shown in Figure 3.2. The light emitted by the fluorescent dye in the laser beam is collected by a Questar QM1 long-range microscope. The microscope's Maksutov-Cassegrain optical system has a clear aperture of 89mm and a 3 micron resolution capability as specified by the manufacturer. The microscope is designed for focusing in a range from 0.559m to 1.956m and is used with the focal distance set at 0.75m, approximately. Magnifications have been varied from 2.1 to 5.0 power in the present work at this distance.

From the microscope, the fluorescent radiation emitted by the dye in the laser beam is focused onto the input window of a Princeton Instruments model IRY-512 single stage microchannel plate image intensifier. A Schott glass long pass filter with a 50% cut-off at 515nm is positioned between the microscope and the input window to eliminate scattered excitation radiation from the signal. The image intensifier provides a luminous gain of at least 10,000 and can be electronically gated open to collect photons for periods from 80 nanoseconds to 7 milliseconds by a high voltage pulse generator. A gate period of 7.17 microseconds is used to limit convection of the fluid through the excitation beam during the integration period, thus resulting in near instantaneous concentration profiles. The gate pulse is provided by a Princeton Instruments model PG-10 pulse generator.

The output P20 phosphor screen of the image intensifier is fiber optically coupled to the input window of a Reticon S series

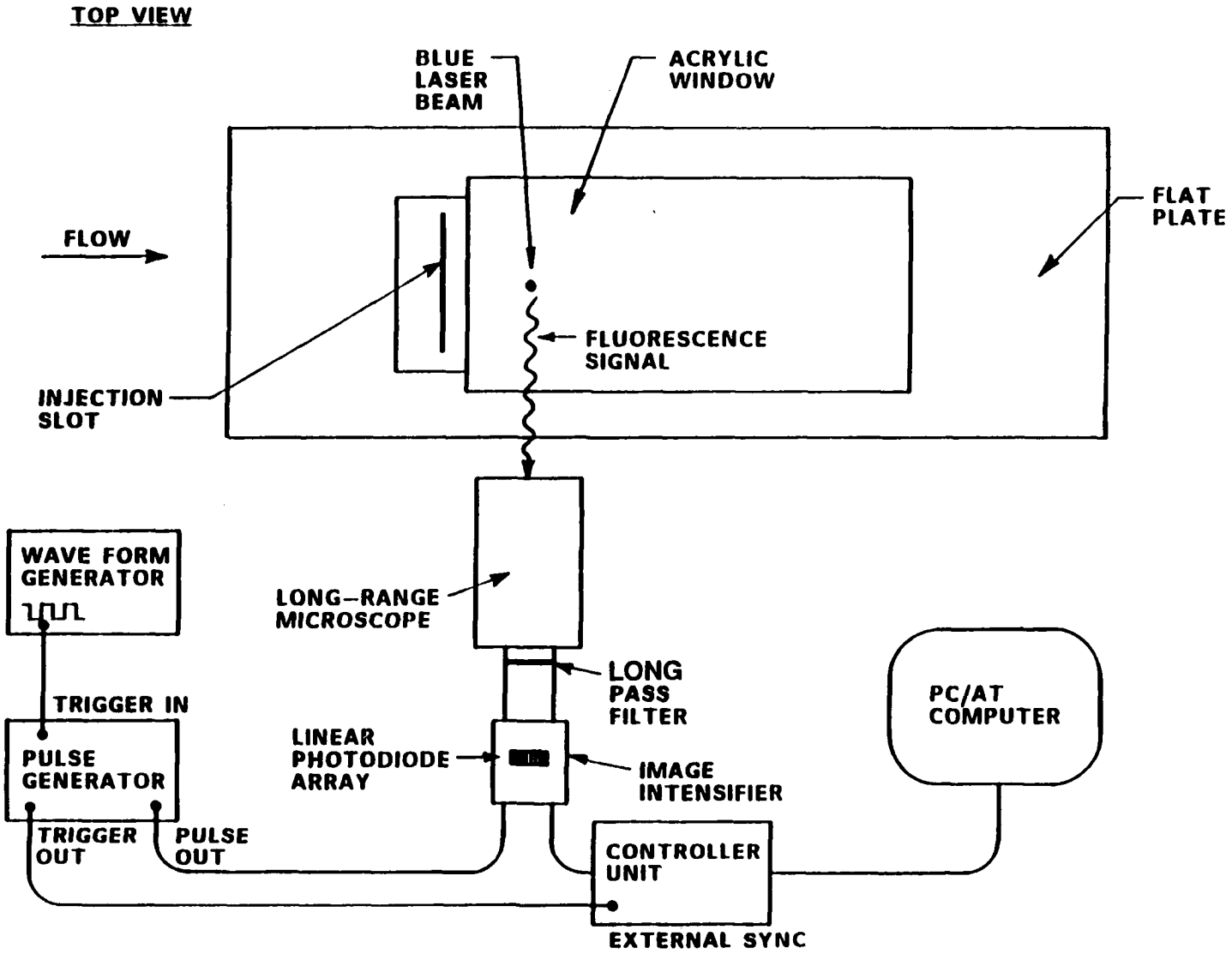

Figure 3.2. LIF Imaging Optics, Electro Optics, and Electronics

512 pixel element linear photodiode array. Since the phosphorescence of the image intensifier's output screen does not decay instantaneously, an image lag between successive scans of the array is possible. This was investigated experimentally by placing a mechanical shutter in the excitation laser beam with the imaging optics focused onto the fluorescence from a uniform concentration dye solution circulating through the calibration flow cell. The mechanical shutter allowed light onto the phosphor screen for a period sufficient for one gating of the array only. Subsequent scans did not have an input signal and as result showed the extent of the suspected image lag.

Figure 3.3 shows the retained image as a function of pixel number for three successive scans after the phosphor screen was exposed to the fluorescent light. The array is scanned serially beginning with pixel 1 and essentially recorded the screen's phosphorescence decay with time. While the retained image in the 2nd and 3rd scans is small, being approximately 2 to 3%, the first scan after exposure recorded up to 45% of the initial image at pixel 3. At pixel 50, however, the retained image is only 15% for the first scan after exposure and continues decaying in an approximately exponential manner with increasing pixel number (i.e., time). The retained image was found to be independent of image brightness and the frequency at which the array is scanned. Therefore, since the first 49 pixels on the array are typically not

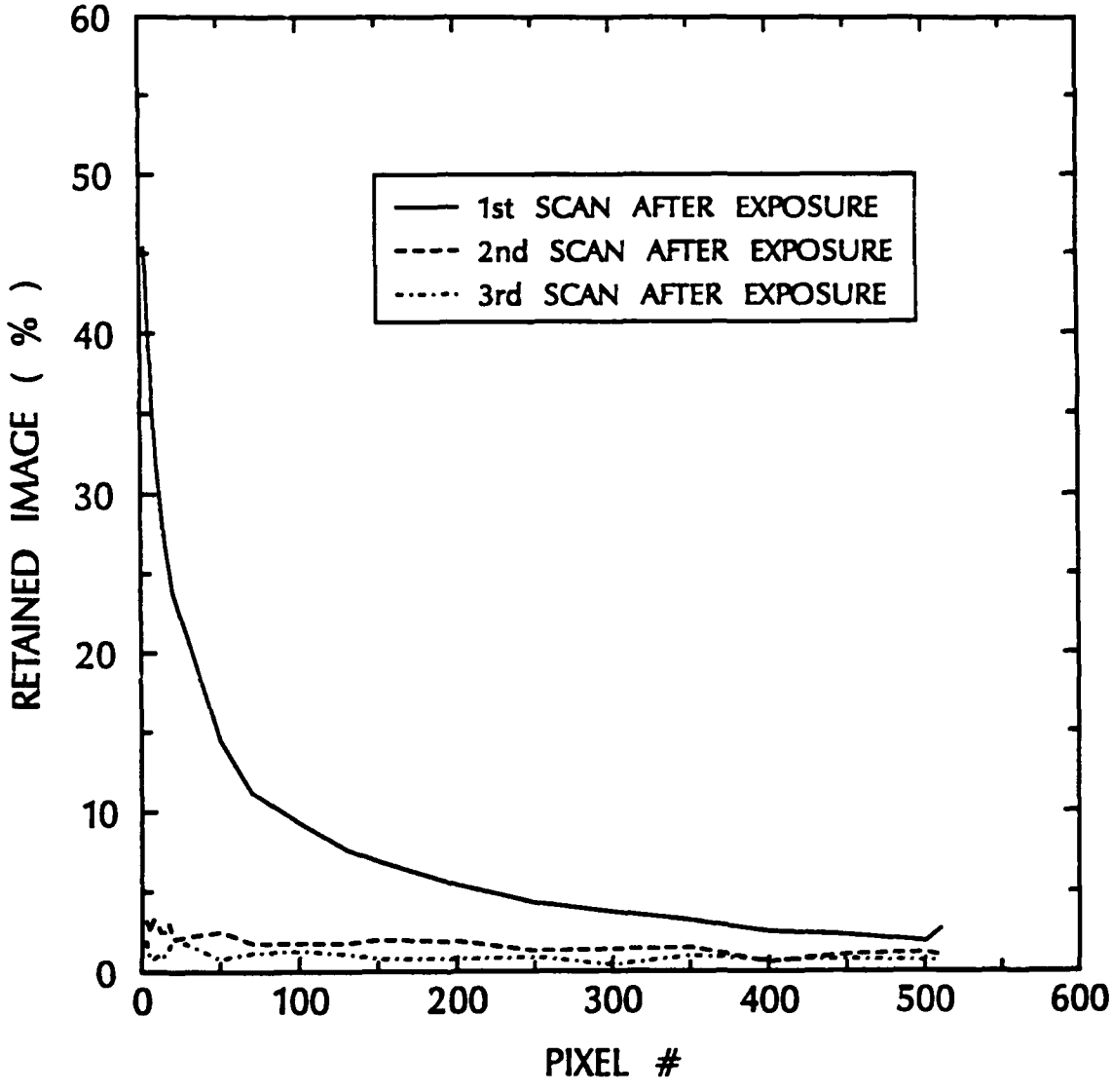

Figure 3.3. Retained Image on the Image Intensifier's Output Phosphor Screen

used in acquiring data, image lag is not felt to be a significant factor influencing the results.

The array pixel dimensions are 25 microns along the axis of the excitation laser beam and 2.5mm perpendicular to the beam axis. The wide 2.5mm dimension of the array pixels allows the entire diameter of the laser beam to be imaged onto the array even with 5x magnification and in the presence of vibration. This avoids possible signal variations resulting from the beam image moving partially off the array.

The analog output signal from the array is directly proportional to the illumination of the image intensifier input window. According to the manufacturer, the sensitivity of the 512 pixel elements can vary up to 20%; however, any sensitivity variations are removed by data processing procedures. Cold tap water is circulated through the intensifier/array system to remove waste heat from a thermonic cooler used to reduce dark noise and photon shot noise by cooling the array to -25 degrees Celsius. Dry nitrogen is blown over the array to prevent condensation. By using short gate periods, the dark noise and photon shot noise may be further reduced and were found by examining the resulting noise from gate periods of various lengths to be negligible. By far, the predominant source of noise is due to the incomplete cancellation of instrumentation clock switching transients. The clock noise,

however, like pixel sensitivity variations, is easily removed in the data processing.

The size of the image viewed by an individual photodiode depends on the microscope magnification along the axis of the laser beam (Y-direction) and on the distance the flow moves in the streamwise direction, X, during one intensifier gate period (see Figure 3.4). At a 4.6m/s test velocity, this X distance is approximately 33 microns. The beam diameter, 90 microns in the current study, determines the resolution in the third coordinate direction Z. In the Y direction at 5x magnification, a 5 micron slice of the laser beam in the flow is imaged onto one photodiode on the array. This equals one viscous wall unit in the TBL at a 4.6m/s test velocity. The resolution of the instrumentation is limited, however, by the image intensifier which has a full width at half modulation of 3 to 3.5 pixels based on the manufacturer's specifications. This limit was verified experimentally by suspending a 25.4 micron diameter wire in the laser beam slightly above and parallel to the plate's surface. At 2.1x magnification, the image of the wire should be viewed by the array as a thin sliver of light only 2 to 3 photodiodes wide with the precise width depending on what portion of the wire's top half is illuminated. Ideally, the resulting output signal from the array would be confined to only the photodiodes illuminated. However, the output signal was a spike three photodiodes wide at the top with a slender base, the signal from the center photodiode falling to half

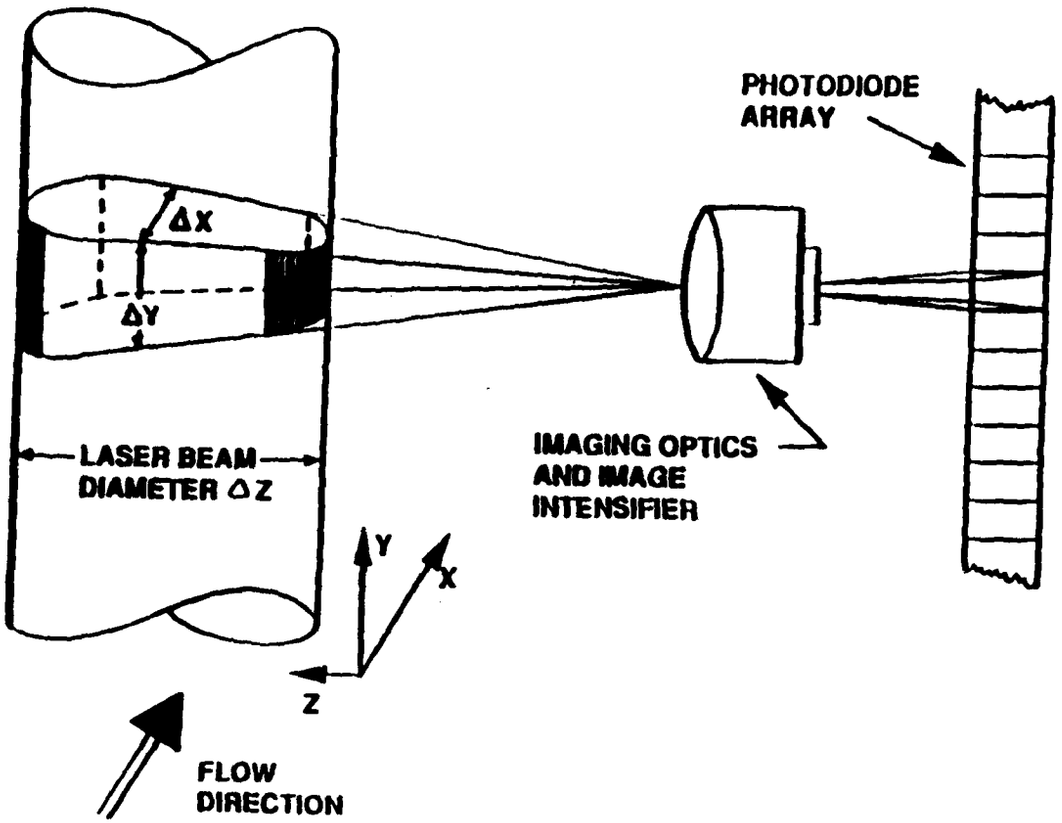

Figure 3.4. Image Viewed by an Individual Photodiode on the Array

amplitude in 2 to 3 pixels (see Figure 3.5). This is partially attributed to the spreading of the electron cloud between the microchannel plate and the output phosphor screen of the image intensifier [see Wick (1987)]. Based on the manufacturer's specifications, blooming in the photodiode array is a relatively small part of this signal spread.

A Princeton Instruments model ST-120 OSM Detector Controller scans and resets the array after each intensifier gate period. The sequence of events leading to the scanning of the array can be described by referring to Figure 3.2 as follows. An Exact Electronics model 7271 waveform generator triggers the pulse generator with a 50 to 60Hz signal. The pulse generator in turn sends a high voltage gate pulse to the image intensifier and at the end of the gate pulse triggers the controller to scan the array. The image intensifier is gated open to collect photons after which the array is scanned. The array is scanned serially across all 512 channels and 50 to 60 array scans are sampled per second. Typically, the array is scanned 1000 times for each test condition, and the resulting data are digitized with a dynamic range from 1 to 16384 and stored on an Everex model EX-2700B personal computer for processing. The computer is equipped with a 12MHz clock and a 72Mbyte hard disk drive. The large amount of disk storage space is necessary since each 1000 scan set produces over 1Mbyte of data. A near real time display on the computer facilitates experiment set-up and monitoring.

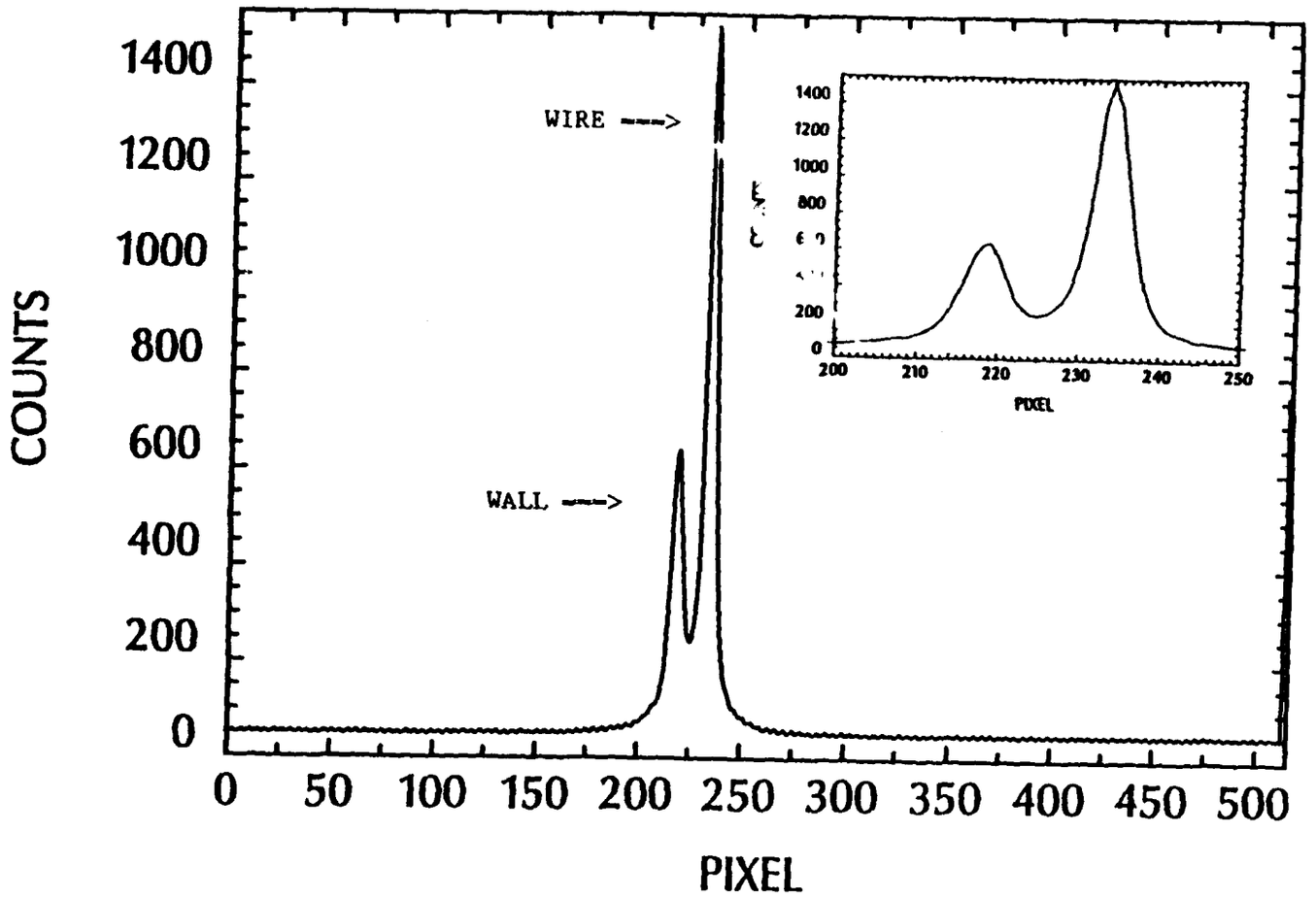

Figure 3.5. System Response to a Light Source Illuminating Two to Three Photodiodes

CHAPTER 4

DATA REDUCTION

4.1 Quantification of the Injectant Concentration

The attenuation of a laser beam passing through a fluorescent dye solution is expressed by the Lambert-Beer law as

$$dI(Y) = - \varepsilon C(Y) I(Y) dY \tag{4.1}$$

where I = laser beam intensity

Y = distance from some reference location (cm)

C = dye concentration (moles/liter)

ε = extinction coefficient (cm x moles/liter)

The extinction coefficient is a function of the particular dye used and of the excitation wavelength. Fluorescein disodium salt was the fluorescent dye used in the current study (see Appendix). Koochesfahani (1984) estimated $\varepsilon = 15700/(\text{cm x moles/liter})$ for a 514.5nm wavelength and Walker (1987) cites a value of 87200/(cm x moles/liter) at 488nm, the current wavelength. Integrating eqn. (4.1) from Y_o to Y yields

$$I(Y) = I(Y_o) \exp \left(-\varepsilon \int_{Y_o}^{Y} C(Y) dY\right) \tag{4.2}$$

The fluorescence intensity emitted over a length ΔY at a point Y along the laser beam may be expressed by Beer's Law as

$$I_f(Y) = QI(Y)\left(1 - e^{-\epsilon \int_{Y}^{Y+\Delta Y} C(Y)dY}\right) \qquad (4.3)$$

where I_f = intensity of the fluorescence

Q = quantum yield of the dye (i.e., the fraction of absorbed photons resulting in fluorescent emission)

In general, the quantum yield Q is a function of dye concentration. However, for fluorescein over the range of dye concentrations used, Q is essentially constant [see Walker (1987) and Pringsheim (1949)]. By assuming an average concentration over ΔY one can write

$$\int_{Y}^{Y+\Delta Y} C(Y)dY = C_A \Delta Y \qquad (4.4)$$

If ΔY is the length of the beam imaged on one photodiode of the array, C_A is what is going to be measured. By substituting eqn. (4.4) into eqn. (4.3), $I_f(Y)$ can be written as follows:

$$I_f(Y) = QI(Y)(1 - e^{-\epsilon C_A \Delta Y}) \qquad (4.5)$$

When $\epsilon C_A \Delta Y \ll 1$, which was always the case in the present study; with $\epsilon C_A \Delta Y = 10^{-4}$ being the largest value used, eqn. (4.5) may be rewritten as

$$I_f(Y) = QI(Y)\epsilon C_A \Delta Y \qquad (4.6)$$

since

$$e^{-x} = 1 - \frac{x}{1!} + \frac{x^2}{2!} - \frac{x^3}{3!} + \frac{x^4}{4!} + \ldots \qquad (4.7)$$

By substituting eqn. (4.2) into eqn. (4.6), one arrives at an alternate expression for the fluorescence intensity from some small slice, ΔY, of the excitation laser beam. When $\varepsilon C_A \Delta Y \ll 1$, this is

$$I_f(Y) = Q\varepsilon\Delta Y I(Y_o) C_A \exp\left(-\varepsilon \int_{Y_o}^{Y} C(Y)dY\right) \qquad (4.8)$$

The signal strength output from a slice of the laser beam imaged onto the i-th pixel element depends on a number of independent factors such as window and lens reflections and imperfections, pixel sensitivity, image intensifier gain, gate period, noise, etc. as well as the local fluorescence intensity (i.e., dye concentration). The output signal of the i^{th} photodiode can then be written as follows:

$$V_i = W_i L_i S_i G_i P_i I_{fi} + N_i \qquad (4.9)$$

where
- V = output signal
- W = window reflections and imperfections
- L = lens reflections and imperfections
- S = pixel sensitivity
- G = image intensifier gain
- P = gate period
- N = noise
- I_f = local fluorescence intensity

By substituting eqn. (4.8) into eqn. (4.9) and dropping the A subscript in C_{Ai}, V_i can be written as

$$V_i = W_i L_i S_i G_i P_i Q \varepsilon \Delta Y I(Y_o) C_i \exp\left(-\varepsilon \int_{Y_o}^{Y} C(Y)dY\right) + N_i \qquad (4.10)$$

The terms other than the noise contributing to the output signal which, in the range of dye concentrations used, are not concentration dependent include W, L, S, G, P, Q, ε, ΔY and, $I(Y_o)$. Rather than trying to account for each factor individually, it is more convenient to lump the factors independent of concentration into a calibration constant A, Koochesfahani (1984). This is of course valid only if the conditions at calibration are the same as during the experiment. Thus eqn. (4.10) may be expressed as

$$V_i = A_i C_i \exp\left(-\varepsilon \int_{Y_o}^{Y} C(Y)dY\right) + N_i \qquad (4.11)$$

where $A_i = W_i L_i S_i G_i P_i Q \varepsilon \Delta Y I(Y_o)$

Letting Y_o correspond to the top surface of the flat plate, eqn. (4.11) can be discretized as follows:

$$V_i = A_i C_i \prod_{j=1}^{i-1} \exp\left(-\varepsilon C_j \Delta Y\right) + N_i \qquad (4.12)$$

The exponential term in the above equations accounts for absorption of the excitation beam by dye over its path to the slice imaged by the i^{th} pixel. Because the field of view of the imaging optics does not always span the entire diffusion layer, absorption outside the field of view could potentially be a factor when higher injection concentrations of dye are used. To avoid this, the excitation beam was directed through the plate as shown in Figure

3.1. With the laser beam directed through the plate perpendicular to its surface, the photodiode array gathers the data required for the discretized exponential term in eqn. (4.12). At sufficiently low dye concentrations and short beam path lengths, however, attenuation can be neglected and eqn. (4.12) may be simplified as follows:

$$V_i = A_i C_i + N_i \tag{4.13}$$

Except at the higher calibration concentrations used, this was always the case in the present work. In all cases, beam attenuation along its path from the tunnel sidewall to the plate due to the buildup of a background dye concentration in the tunnel was negligible.

4.2 Calibration

Calibration involves relating the fluorescence from a known concentration dye solution to the resulting digitized output signal from the microscope/intensifier/array system. Analytically this requires solving (4.12) for A_i using measured values of V_i for a known value of C_i, and N_i without an input signal. N_i can also contain that portion of the signal resulting from a build-up of a background dye concentration in the tunnel. For a uniform concentration dye solution, the i and j subscripts may be dropped from C and solving (4.12) for A_i yields the following calibration equation:

$$A_i = \frac{(V_i - N_i)}{C \prod_{j=1}^{i-1} \exp(-\epsilon C \Delta Y)} \qquad (4.14)$$

The calibration procedure is to fill the tunnel until the water level is slightly above the top surface of the flat plate. A small calibration flow cell is then placed in the test section at the measurement location of interest. The cell, shown in Figure 4.1, has no bottom surface and seals against the acrylic window of the test plate when weights are placed on top of it. A small high speed pump is used to circulate the calibration fluid and a schematic of the flow cell pumping system is shown in Figure 4.2. The flow rate through the cell is quite high to eliminate possible errors due to photobleaching and thermal blooming (see Appendix). Thus, the calibration is performed with the excitation and imaging optics set-up exactly as they are for the experimental measurements to follow except that reflections off the window on the calibration cell are not accounted for. Transmittance calculations, however, show that the loss of signal resulting from these reflections is negligible; being approximately 0.6%. The signal loss was also experimentally found to be negligible by comparing the fluorescence signal measured from a dye solution in the calibration flow cell with the flow cell window in place to the signal measured with the window removed. The procedure used is discussed below.

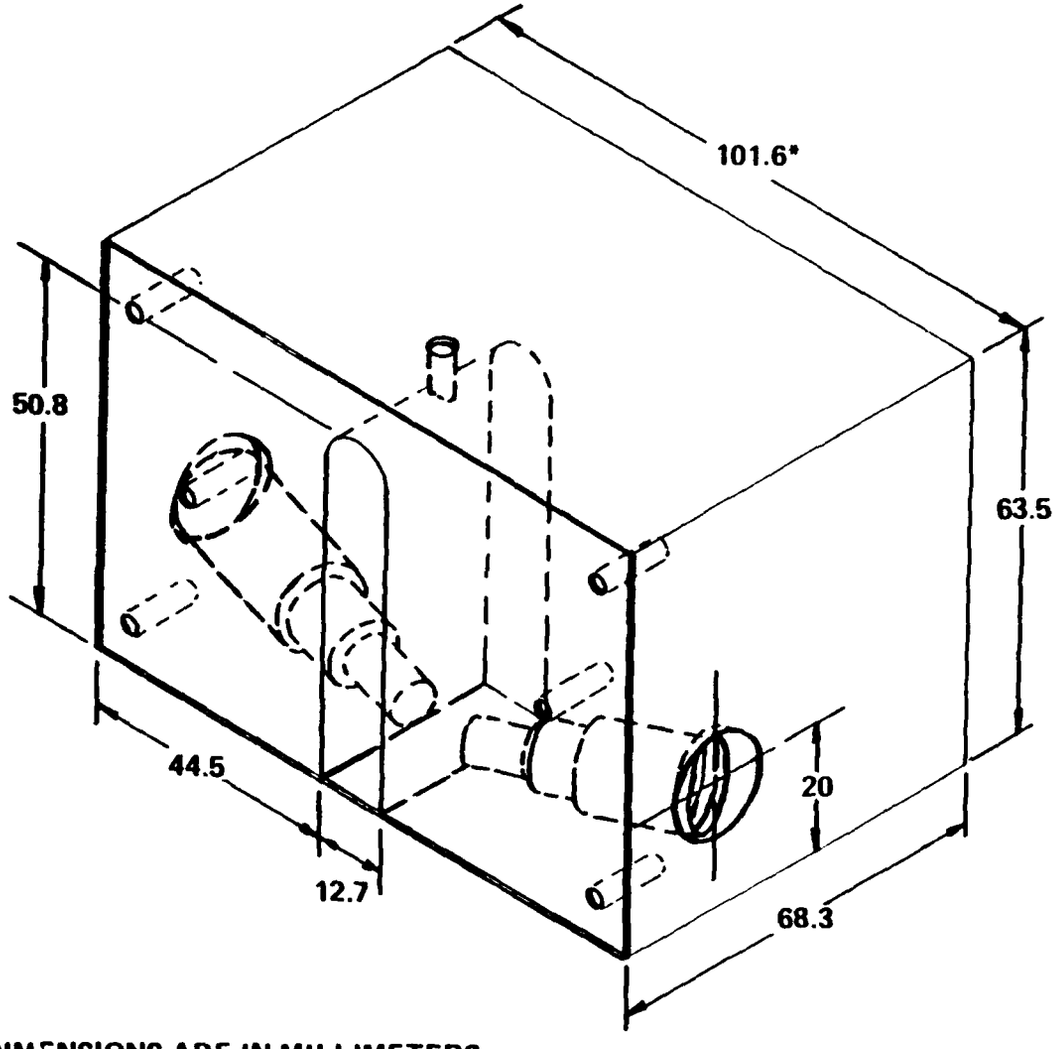

*ALL DIMENSIONS ARE IN MILLIMETERS

Figure 4.1. The Calibration Flow Cell

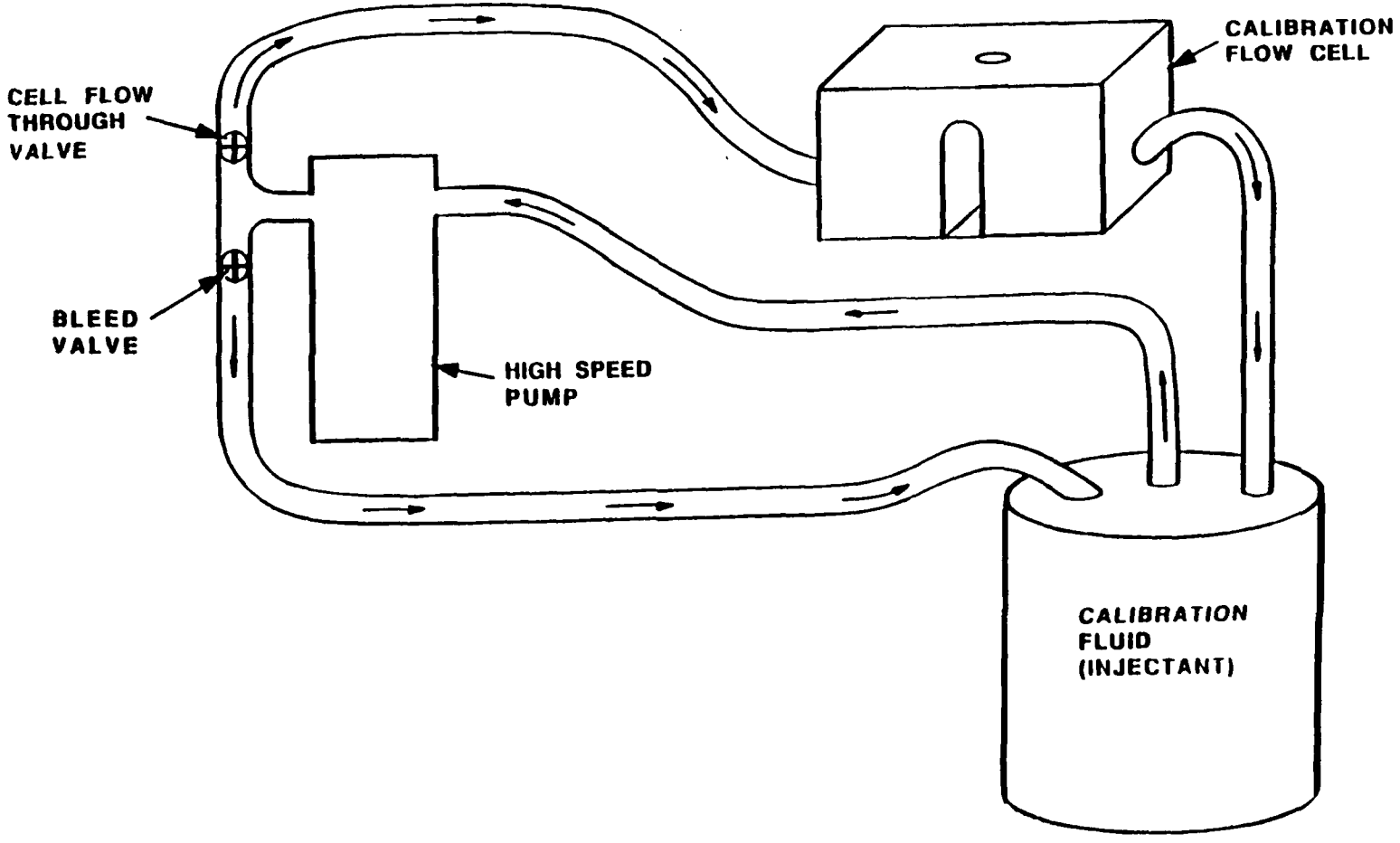

Figure 4.2. Schematic of the Calibration Flow Cell Pumping System

The tunnel was filled with water and dye was added until the concentration was 2 x 10^{-8} moles/liter. The tunnel volume was determined by dissolving 500g, 1000g, and 2000g of sodium sulfate in the tunnel and comparing the resulting changes in the water conductivity with a reference solution. The three values obtained for the tunnel agreed within 0.01%; the tunnel volume being 15,400 liters. The tunnel was then drained until the dyed water level was slightly above the top surface of the plate. In order to determine the attenuation caused by the flow cell window, the flow cell was installed, dyed tunnel water was circulated through it, and data were taken. To provide a baseline for comparison, the flow cell window was then quickly removed and with the LIF instrumentation set-up exactly as it was for the preceding measurements, dyed tunnel water was again circulated through the flow cell and data were taken. The measurements taken with the flow cell window in place were within 1% of the measurements taken with the window removed.

In order to compare the measurements taken with the flow cell window in place to those taken with the window removed, it was necessary that the two data sets be taken over a short period of time. This is because the fluorescence intensity of solutions of water and fluorescein was observed to diminish with time. Fluorescein does not fluoresce in an oxidized state and is an effective indicator of oxidatation reduction reactions, Guilbault

(1973). It appears that the dye may be reacting with dissolved substances in the water. The fluorescence decay of solutions made with fluorescein and polymer was not as rapid. Initially, dye was added to the injectant immediately prior to use to avoid these signal decay effects. However, since the fluorescence signal decay rate was observed to diminish appreciably with time, the use of aged solutions was adopted. This produced better repetition of the calibrations than the former procedure.

The fluorescence intensity of fluorescein is dependent on the fluid in which the dye is dissolved (see Appendix). Thus, it is necessary to calibrate with the fluid which is to be injected into the TBL through the slot. Calibrations are taken at dye concentrations ranging from the injection concentration to 1/32 or 1/64 of the injection concentration. These multiple concentration calibrations are done to verify the expected linear variation of the signal with concentration and to provide some experimental estimate of the error that is likely in the TBL concentration profile measurements. Figure 4.3 shows the pixel sensitivity in counts per (mole/liter) of dye versus dye concentration for water at four pixels on the array for a typical set of calibrations. The sensitivity of a given pixel should be constant, and the variations about the mean are less than 10%. This is reasonably good considering that the calibration concentrations are estimated as 5% accurate. The calibration solutions of both water and polymer are

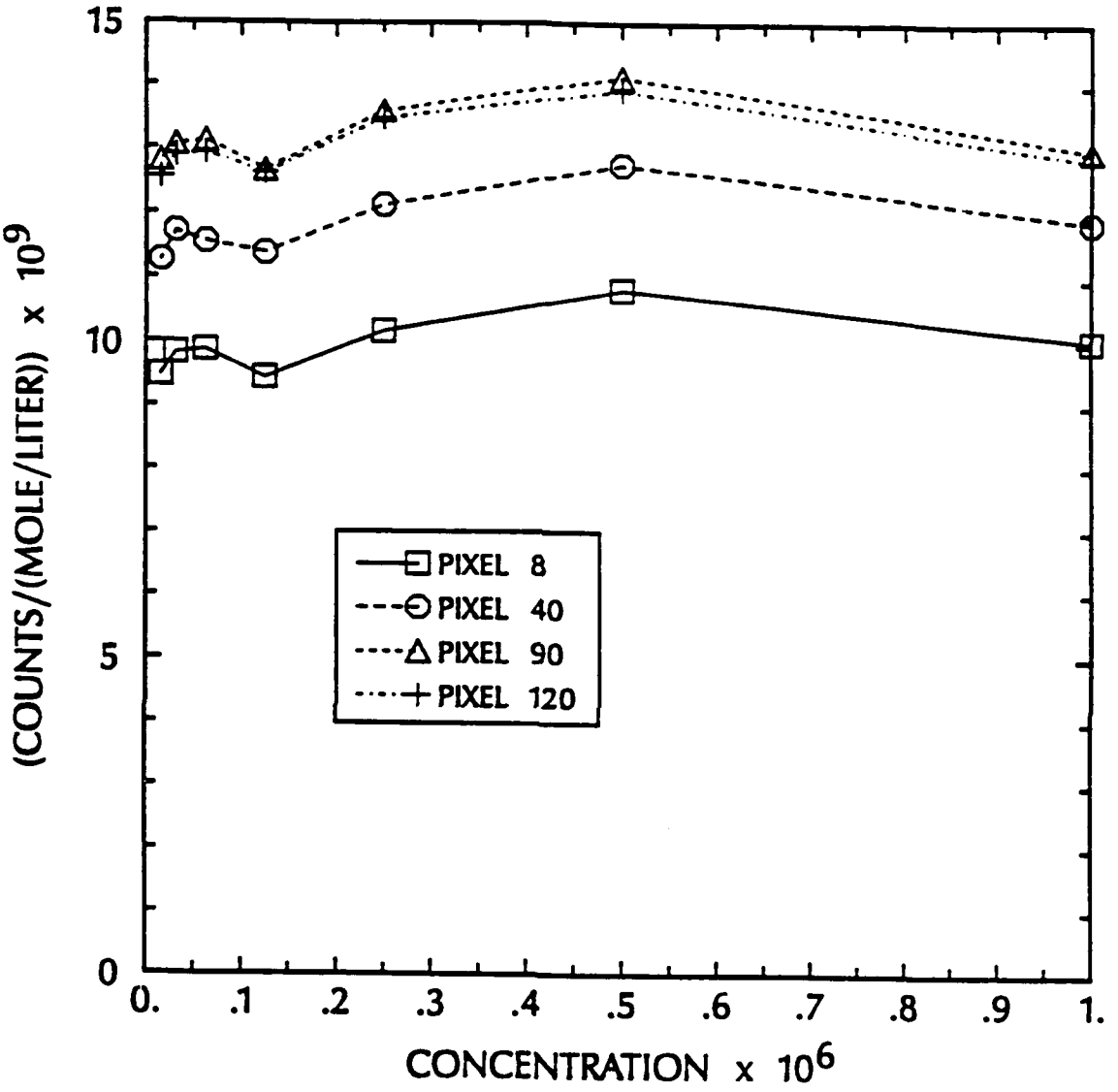

Figure 4.3. Pixel Sensitivities Determined From Flow Cell Calibrations for a Range of Dye Concentrations

diluted to their respective concentrations with tunnel water to simulate the actual diffusion process as accurately as possible. The major difficulty with this flow cell procedure is that bubbles attach themselves to the cell window in the near wall region and must be carefully removed. Also, when calibrating with the more viscous polymer solutions, bubbles in the flow can somewhat decrease the measured signal, particularly far from the wall. In general, however, if proper care is taken to minimize bubbles in the flow, the calibration data statistics at a given pixel are Gaussian with the standard deviation ranging from approximately 6.5% of the local mean at the lowest calibration concentration used to 10% of the local mean at the highest calibration concentration used.

To examine how well the calibrations taken with the calibration flow cell represents the signals obtained with an actual flow inside the tunnel, the following simple experiment was performed. The tunnel was filled with water, and dye was added until the concentration was 2×10^{-8} moles/liter. Data were taken with the dyed water being circulated through the tunnel. The tunnel was then drained until the water level was slightly above the top surface of the plate. The flow cell was installed, and dyed tunnel water was circulated through it. Data were taken with the LIF instrumentation set-up exactly as it was for the tunnel as a flow cell measurement. Due to the fluorescence decay during the

time interval between measurements, it is not possible to compare directly the magnitude of the averaged profiles, however, it is possible to compare the shapes. Figure 4.4 shows the averaged output signal from the array for both measurements normalized by the averaged output signal from 6 pixels on the array. Figure 4.5 is a close-up of the near wall region in Figure 4.4. The agreement is excellent. Figures 4.4 and 4.5 show that indeed a useful calibration (in shape) can be obtained with the calibration flow cell even though the flow inside the cell is not a flat plate TBL flow as is present inside the tunnel.

While a strong case has been built justifying the validity of this LIF technique for measuring the injected dye concentration in a TBL, a point which remains to be addressed is the validity of determining the injectant concentration from the measured dye concentration. The injectant concentration is determined directly from the measured dye concentration through the known pre-injection injectant to dye concentration ratio. The argument justifying this relationship is based on the physical properties of a turbulent flow, and the fact that the dye is completely dissolved and intimately mixed into the injectant solution.

Although there is no precise definition of just what a turbulent flow is, all turbulent flows share several common characteristics. Those characteristics relevant to this discussion are that turbulent flows only occur at large Reynolds numbers, are

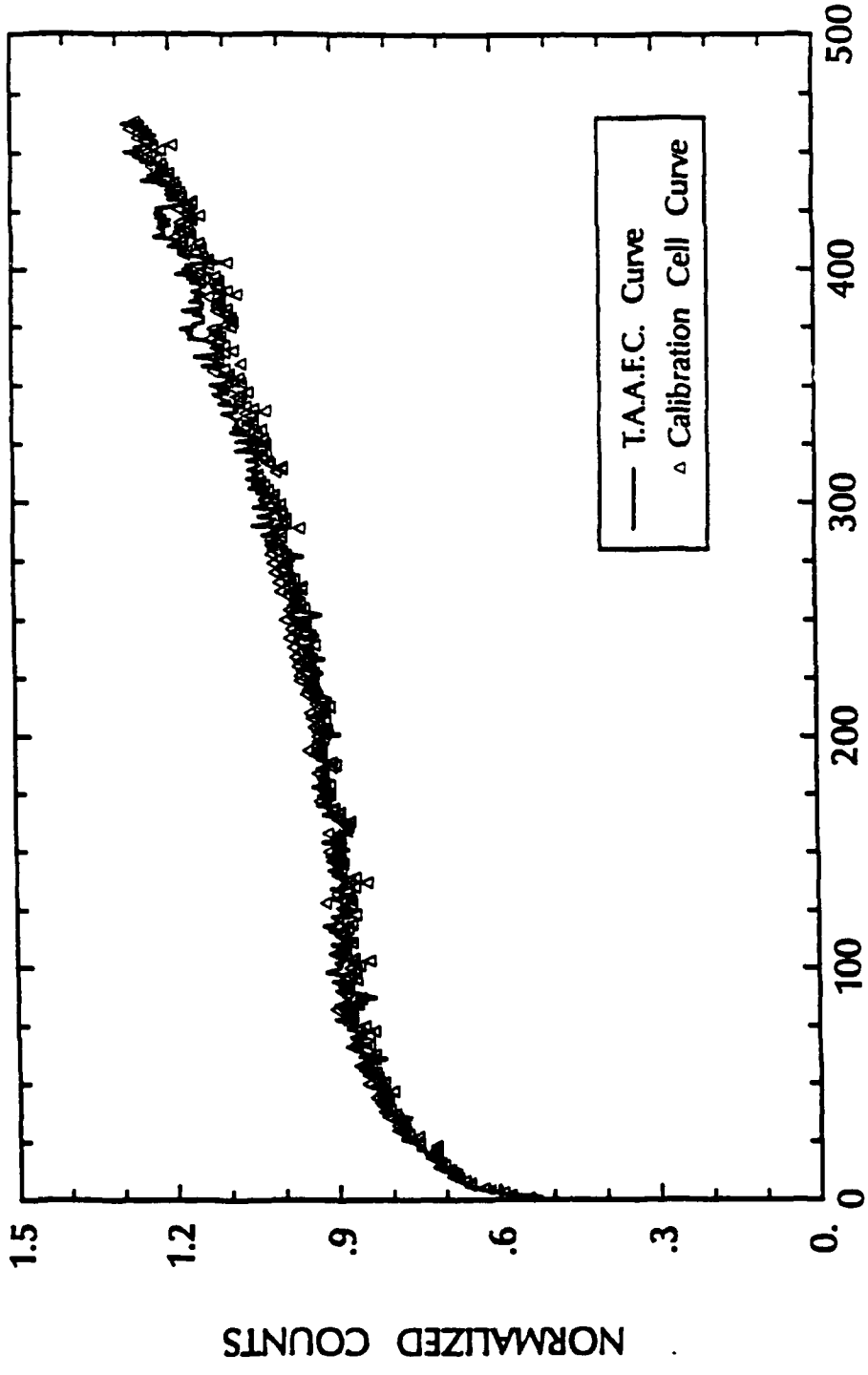

Figure 4.4. Comparison of Normalized Calibration Cell Curve to Normalized Tunnel as a Flow Cell Curve

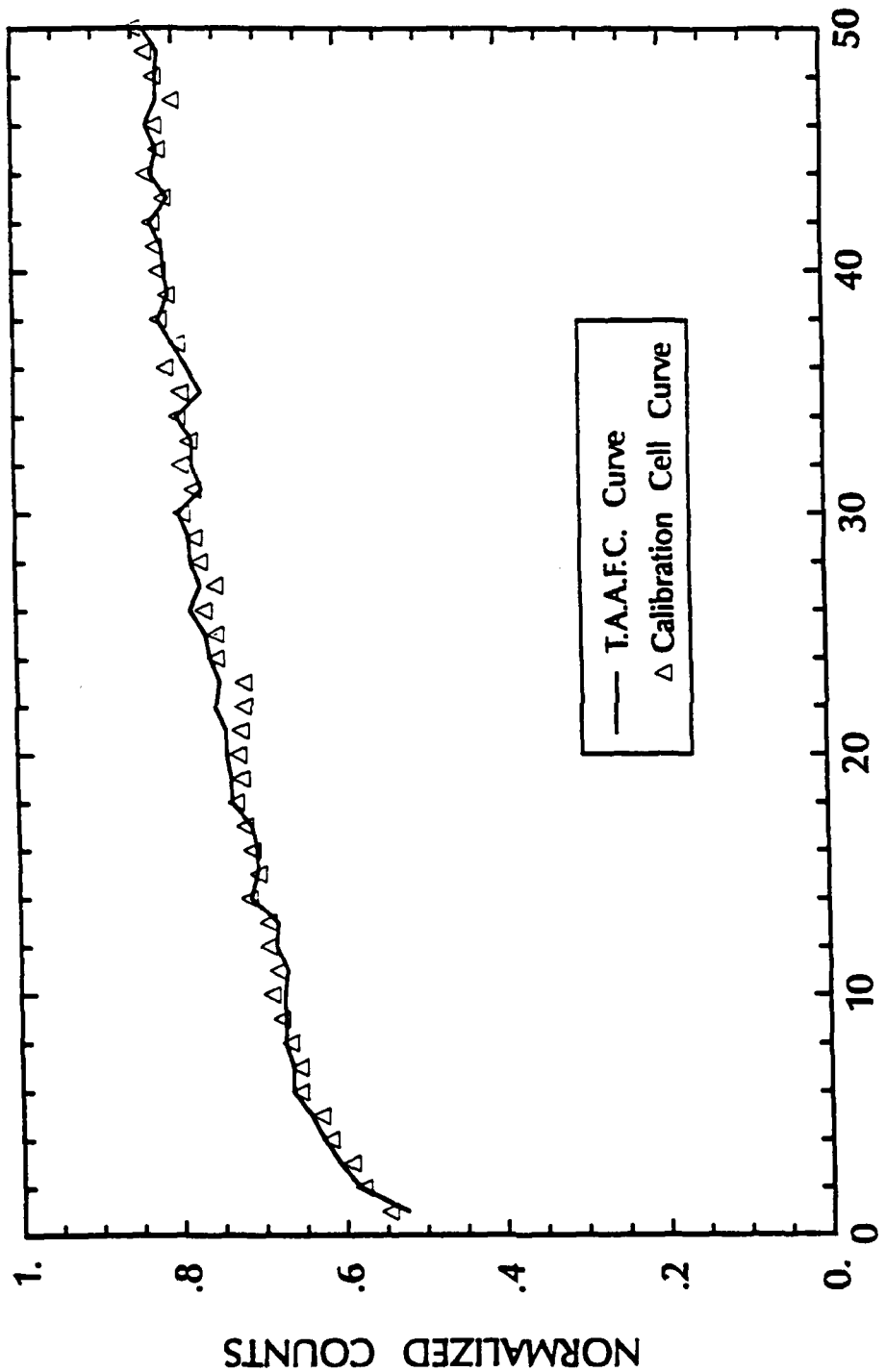

Figure 4.5. Comparison of Normalized Calibration Cell Curve to Normalized Tunnel as a Flow Cell Curve in the Near Wall Region

characterized by three-dimensional random vorticity fluctuations, and have the ability to effectively diffuse mass and momentum. Depending on the Reynolds number, turbulent diffusion is typically orders of magnitude larger than molecular diffusion. Since the Reynolds numbers of the subject flows are high, diffusion occurs almost entirely by turbulent mechanisms. More specifically, the larger size eddies are responsible for most of the large-scale diffusion and the smaller eddies fill in the concentration gaps left by the large scale motions. This turbulent diffusion process via random eddy motion is in no way selective of the molecules that it diffuses. In other words, the turbulence will diffuse injected polymer molecules or water molecules just as effectively as dye molecules. Thus, the turbulence diffuses the dye and injected polymer identically. The flow's lack of selectivity is the justification for determining the injectant concentration via the measured dye concentration.

An implication of the above discussion is that the maximum possible spatial resolution of this technique must be limited by the Kolmogorov length microscales of the flow. At scales smaller than the Kolmogorov microscales, the diffusion of the injectant is not precisely represented by the diffusion of the dye due to the differing molecular diffusivities, D(cm^2/sec), of the injectants and the dye into water ($D_{water} = 1.7 \times 10^{-5}$, $D_{polymer(polyox)} < 10^{-12}$, $D_{dye(fluorescein)} = 5.2 \times 10^{-6}$). At the length scales at which molecular

diffusion is important, dye is not diffused as efficiently as the injected water, but it is diffused far more efficiently than the polymer. The only way for the diffusion of the dye to precisely represent the diffusion of the injectant at scales smaller than the smallest turbulent length scales is for the dye and the injectant to have identical molecular diffusivities (into water). Therefore, only for length scales larger than the Kolmogorov length microscale do the dye and polymer concentrations remain proportional at the pre-injection concentration ratio as they mix with the boundary layer flow.

In summary, the near instantaneous injected dye concentration may be accurately measured by the technique discussed in this thesis. Determining the injectant concentration from the measured dye concentration is valid at length scales larger than the Kolmogorov microscales of the flow. Thus, the limiting spatial resolution of this LIF technique for measuring the injectant concentration is the flow's local Kolmogorov length microscales. For the high unit Reynolds number flat plate flows of interest the local Kolmogorov length microscales, $\eta(X)$, are very small and vary as $\eta(X) \simeq \delta(X) \times (Re_x)^{-3/4}$ [Tennekes and Lumley (1972)]. An empirical relation given by White (1974) for $\delta(X)$ on a flat plate is $\delta(X) \simeq 0.37 \times X \times (Re_x)^{-1/5}$. Therefore, $\eta(X)$ varies approximately as $\eta(X) \simeq 0.37 \times X \times (Re_x)^{-1}$. This implies that as the local Reynolds number increases so does the maximum possible spatial resolution of this LIF technique (i.e., in absolute terms).

CHAPTER 5

CONCENTRATION PROFILE MEASUREMENT PROCEDURE

5.1 How the Measurements Are Performed

Concentration profile data are taken at each measurement location according to the following procedure. The tunnel is filled until the water level is approximately 5cm above the plate's top surface. The laser beam is then adjusted so that its waist is at or slightly above the surface, and the long pass filter, shown in Fig. 3.2, is removed from the optical pathway of the LIF imaging system. The microscope/intensifier/array system is focused using a precision metal ruler as a target and the near real time display on the computer. The surface of the ruler, which is graduated every 0.397mm, is carefully placed in the laser beam perpendicular to the plate with the graduations facing the microscope. The graduations on the ruler scatter the laser light. On the near-real time display each graduation is seen as a spike and the space between each graduation is seen as a narrow valley. The microscope's focusing knob is adjusted until the spikes and valleys reach their maximum amplitude on the computer screen. The quality of the focus could also be judged by the sharpness of the signals from 488nm excitation radiation scattered off bubbles and particles convected through the laser beam. The system magnification was determined by counting the number of pixels separating individual graduations on

the ruler.

Once focused, the calibration flow cell is placed at the measurement location of interest. The location of the plate's surface or wall on the array is also found using the near real time display. Laser light is scattered where the beam passes through the plate's surface with the scattered light at the wall appearing as a sharp spike on the near real time display. In order to verify that this spike indeed represents the wall, a very thin wire, 25.4 microns in diameter, was placed in the laser beam slightly above and parallel to the wall. The two sharp spikes shown in Figure 3.4 were displayed on the computer; one representing the wall and the other the wire above the wall. As the wire was brought to the plate surface, the top spike merged with the bottom wall spike. Thus, the sharp wall spike does indeed represent the location of the wall on the array. The height of the array is adjusted relative to the plate until the wall is positioned at pixel 49 for calibration and concentration profile measurements. Uncertainty as to the precise location of the wall on the array is estimated as at most +/- 2 pixels.

With the LIF instrumentation set-up exactly as it is to be configured for the concentration profile measurements to follow, the calibration fluid is circulated through the flow cell and data are taken. After the calibration procedure has been completed, the flow cell is removed, the tunnel is then sealed and filled with

water. The tunnel is pressurized to 207kPa while running to minimize the size of trapped air bubbles passing through the laser beam and to suppress plate leading edge cavitation at higher operating velocities. Typical test velocities ranged from 4.6m/s to 9.1m/s. Vibration of the plate surface as viewed by the photodiode array was limited to a maximum +/- 1 to 2 pixels at the highest test velocity of 9.1m/s. Polymer or water is injected into the TBL through the slot and data are taken. The calibration of the pump supplying the injectant to the slot is verified periodically.

The polymer used in this study was polyethelene oxide (polyox) with a mean molecular weight, as reported by the manufacturer, of 5×10^6. Polyox was mixed into tap water that had been allowed to sit for a period of at least two days to reduce possible chlorine degradation effects. The polymer was gently stirred every few hours after it was added to the water and was given at least 18 hours to hydrate. Dye was then added and the solution was allowed to sit an additional 24 hours before use. Dyed water solutions were prepared in a similar manner. This minimum 24 hour period allowed the fluorescence decay rate to decrease to the point where it was not a factor in calibration or in performing the concentration profile measurements. Typical injection dye concentrations ranged from 1×10^{-6} to 4×10^{-6} moles/liter.

Injection flowrates are normalized by the flowrate in the viscous sublayer of the pure water boundary layer, Q_s, defined by Wu and Tulin (1972) as the flow through the area extending from the wall to $Y^+ = 11.6$. This sublayer flowrate per unit span is 67.3 times the kinematic viscosity of the fluid. This is an interesting result in that the edge of the sublayer, in the mean, is a streamline and the sublayer flowrate is not a function of velocity. Q_s is approximately 4.05 liters/minute/m span in water at room temperature.

CHAPTER 6

RESULTS

6.1 Water Injection Results

Water was injected into the TBL with freestream velocities of 4.6 and 9.1m/s at flow rates from 2 to $10Q_s$. Mean concentration profiles at the most upstream measurement location, 12.7mm from the slot, at both velocities are shown in Figures 6.1 and 6.2. The microscope magnification was 2.20x and each pixel on the array covered 2.14 viscous wall units vertically at 4.6m/s and 4.04 wall units at 9.1m/s. The maximum possible spatial resolution of the LIF technique is limited however, as mentioned earlier, by the Kolmogorov length microscales of the flow. In the current study, these scales are of the same order of magnitude as the instrumentation resolution normal to the wall.

Near the slot, at the lowest freestream velocity and highest injection rate tested, the diffusion of the injectant should be minimal, and the maximum measured concentration should approach the injection concentration. This serves as a check on the accuracy of the calibration's magnitude. Figure 6.1 shows that at the $10Q_s$ injection rate the ratio of maximum measured concentration to injection concentration is 1.024, implying an error in the calibration at the wall of approximately 2.4%.

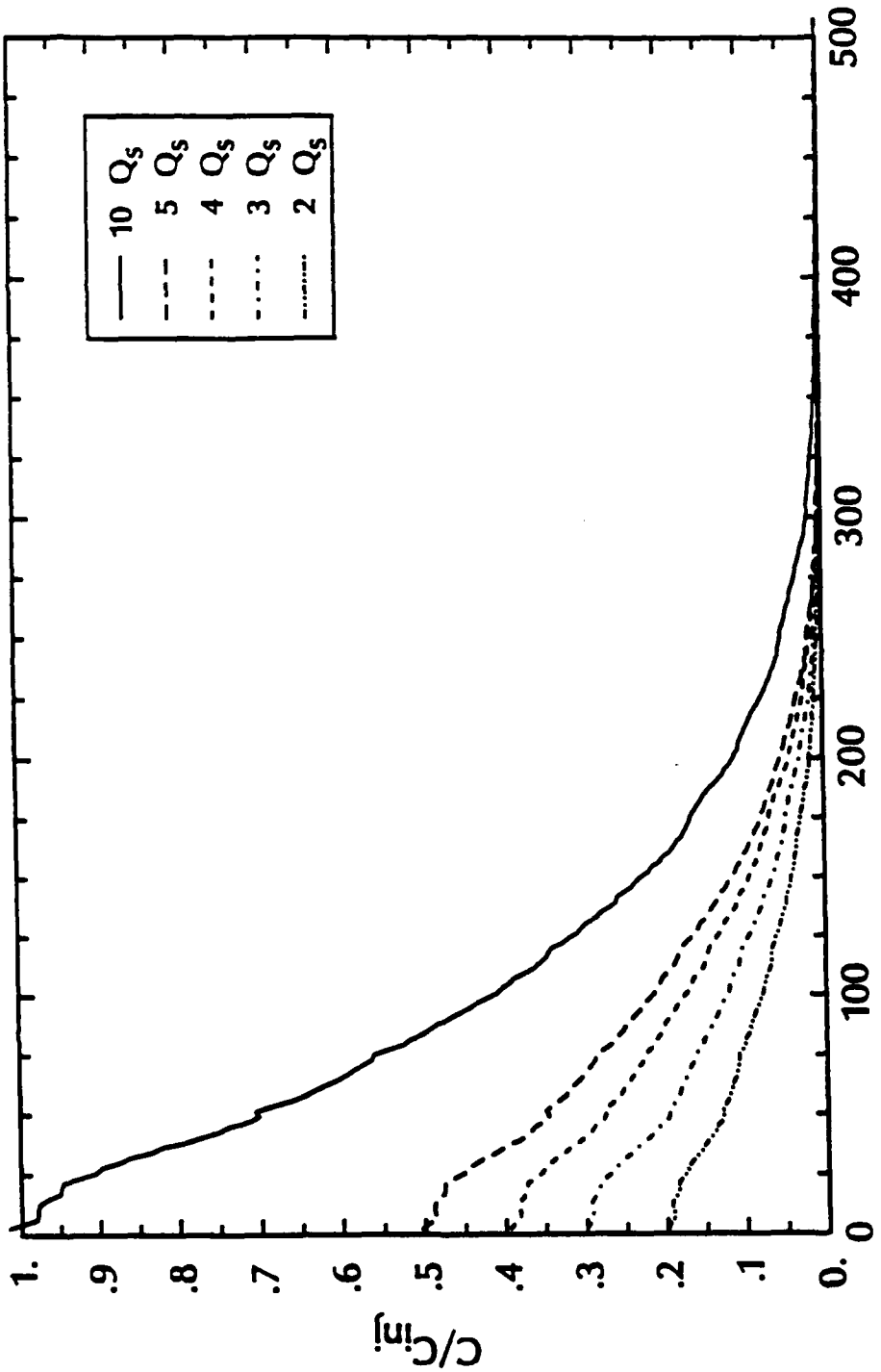

Figure 6.1. Dyed Water Mean Concentration Profiles at U= 4.6m/s, X= 12.7mm

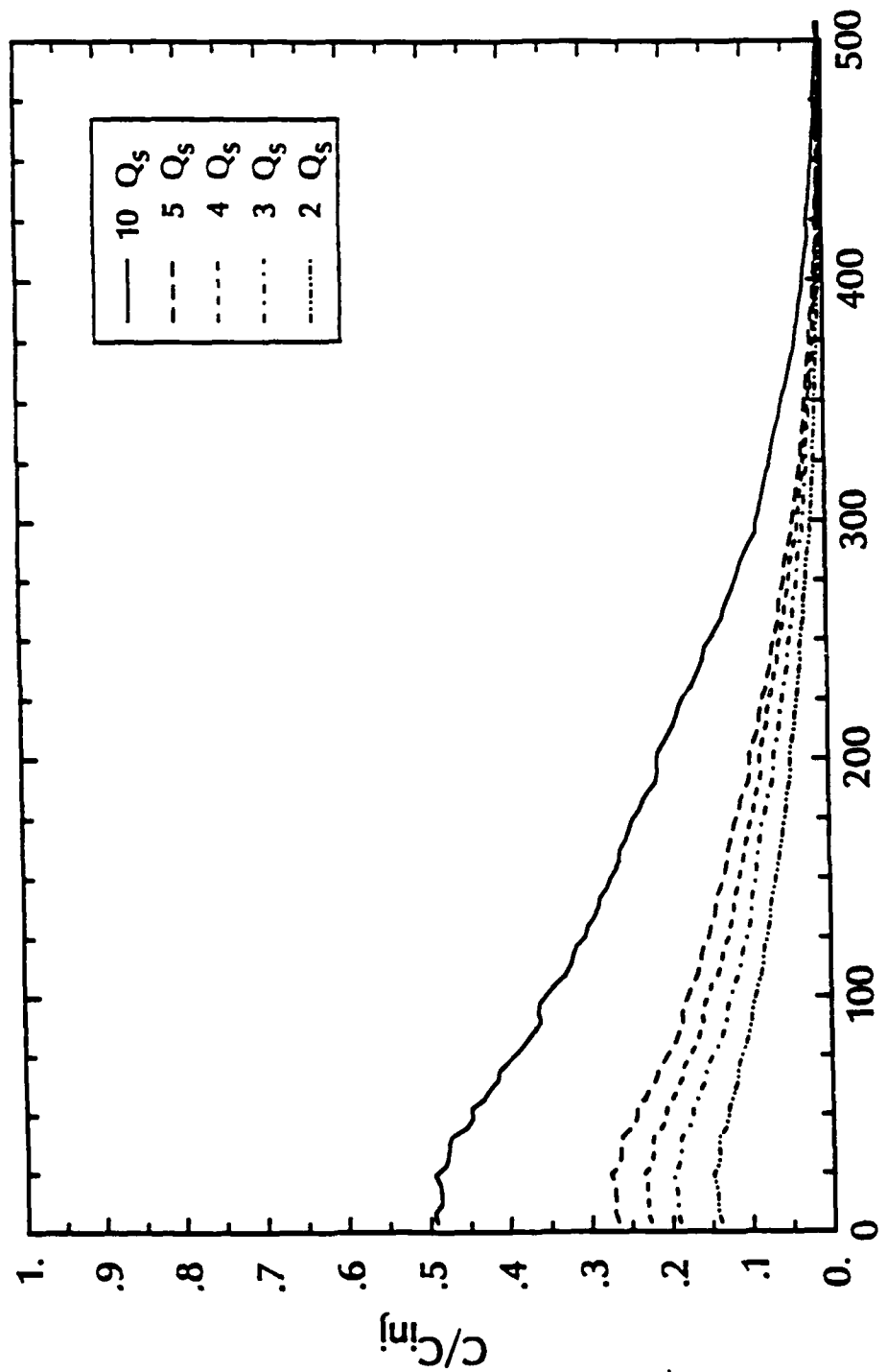

Figure 6.2. Dyed Water Mean Concentration Profiles at U= 9.1m/s, X= 12.7mm

At both velocities, the maximum measured concentration occurs at the wall. For injection rates and distances downstream of the slot where the wall flow is not saturated with pure injectant, the maximum measured concentration is directly proportional to the injection rate and varies inversely with the free stream velocity. This is in agreement with the passive contaminant line source diffusion results of Poreh and Cermak (1964). A diffusion layer thickness, λ, defined as the height above the wall that the mean concentration decreases to 50% of its maximum value at the measurement streamwise position was determined from mean concentration profiles. Figures 6.3 and 6.4 show these λ at 4.6 and 9.1m/s respectively, normalized by local boundary layer thickness, δ_{loc}, versus the streamwise distance from the slot, X, normalized with the average boundary layer thickness between the slot and X, δ_{av}. The solid curves in Figures 6.3 and 6.4 represent the results of Poreh and Cermak (1964) and the agreement with the present results is excellent. These data span what Poreh and Cermak (1964) term the intermediate and transitional diffusion zones. The most downstream measurement location is slightly upstream of the final diffusion zone.

The intermediate zone extends to $X/\delta_{av} = 18$ where $\lambda/\delta_{loc} = 0.39$ approximately. In the intermediate zone the thickness of the diffusing plume is small compared to the boundary layer thickness but large compared to the viscous sublayer thickness and the

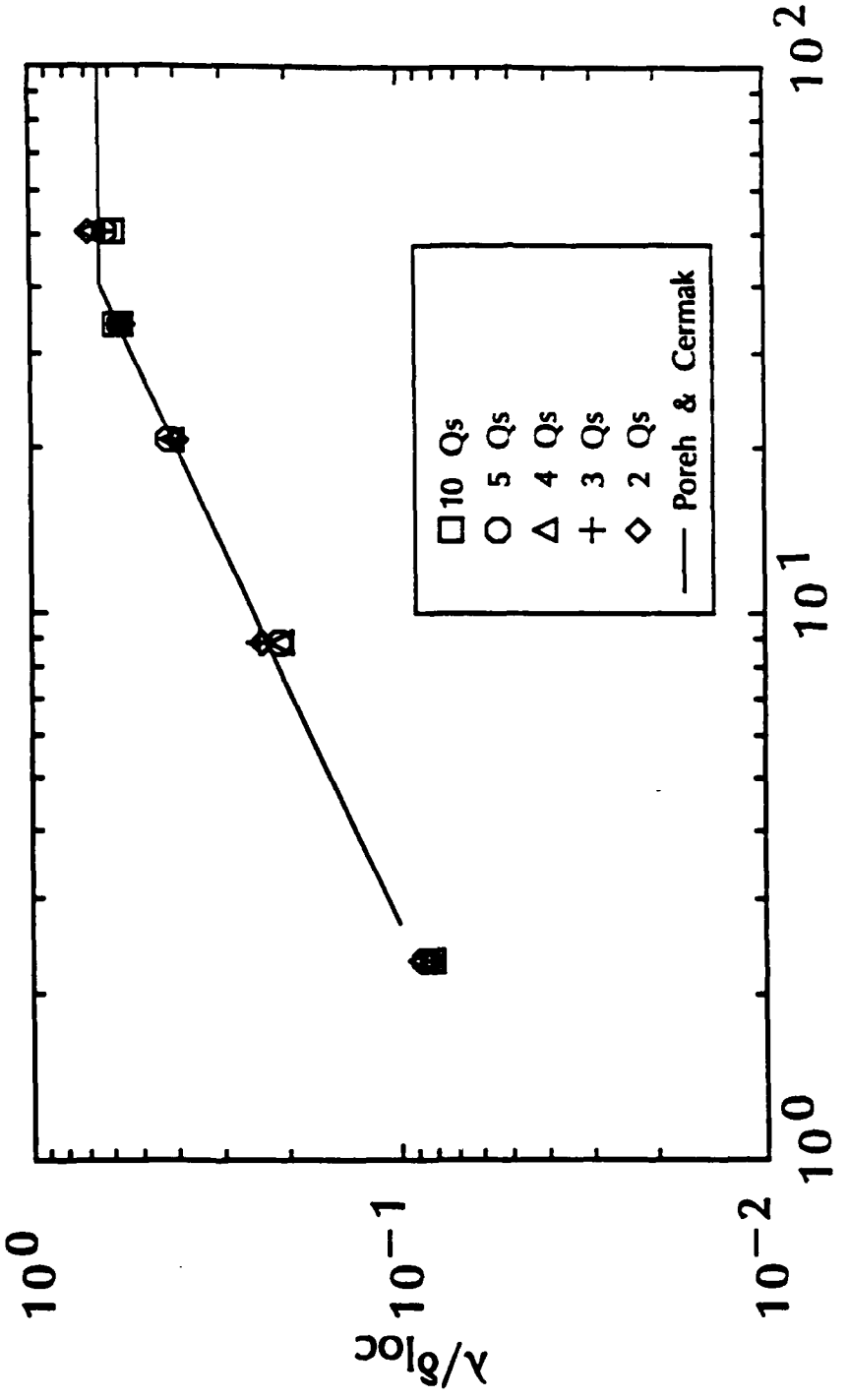

Figure 6.3. Diffusion to Viscous Boundary Layer Thickness Ratio Versus Streamwise Position With Water Injection, U= 4.6m/s

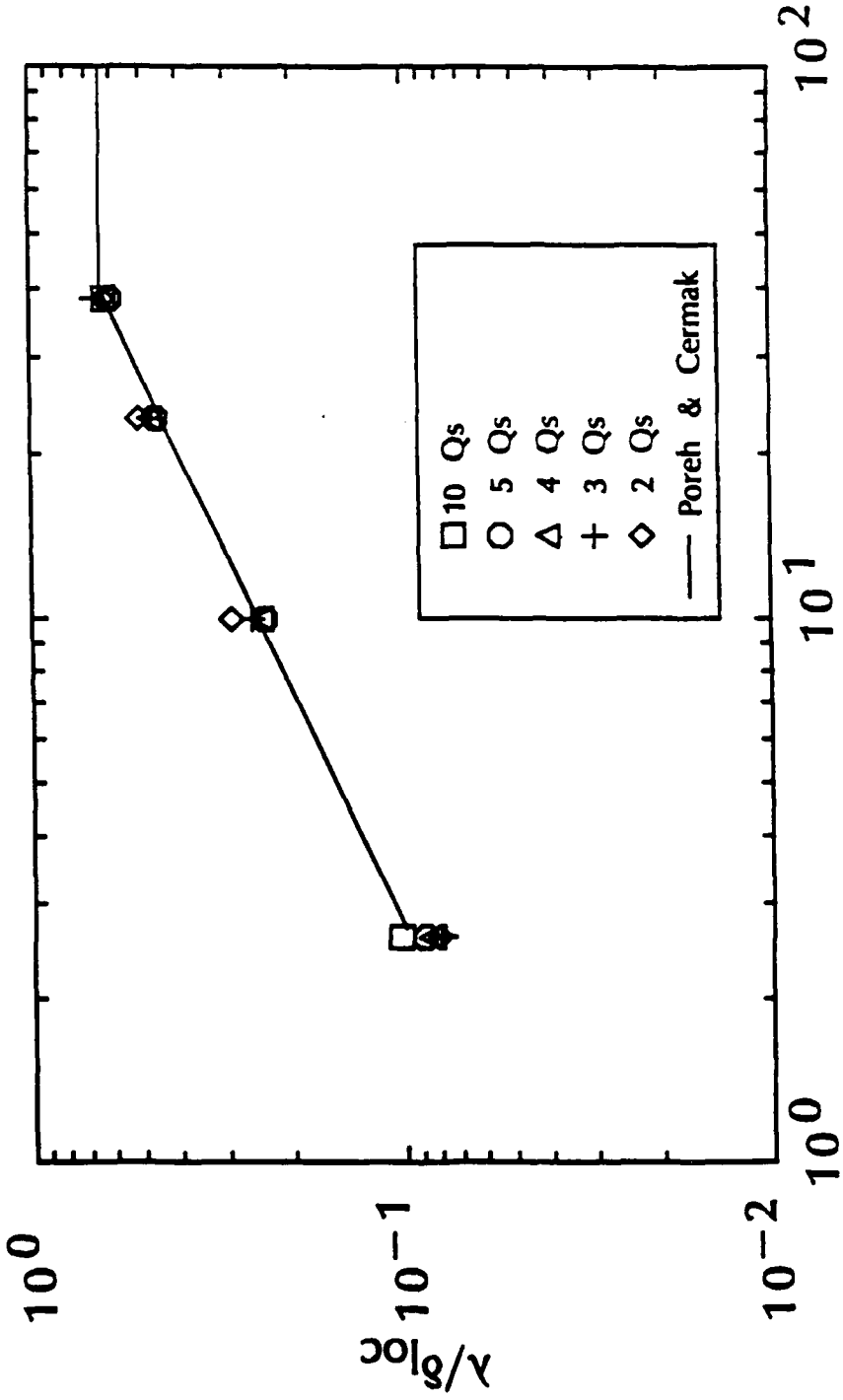

Figure 6.4. Diffusion to Viscous Boundary Layer Thickness Ratio Versus Streamwise Position With Water Injection, U= 9.1m/s

plume's vertical rate of growth is large compared to that of the boundary layer. The transition zone extends from $18< X/\delta_{av} <60$ downstream of which final zone behavior ensues. Through the transition zone, the diffusing plume grows but at a progressively slower rate until its thickness is proportional to the thickness of the boundary layer in the final zone. In the final zone, both the diffusion layer and the viscous boundary layer grow at the same rate, and λ/δ_{loc} remains constant at 0.64.

Mean concentration profiles are approximately invariant in the intermediate and final diffusion zones and can be described by the empirically derived exponential curve of Morkovin (1965) where

$$C/C_{max} = \exp(-0.693(Y/\lambda)^a) \qquad (6.1)$$

and $a = 1.50$ in the intermediate diffusion zone

$a = 2.15$ in the final diffusion zone

At 4.6m/s the most upstream measurement location, 12.7mm from the slot, is located in the intermediate diffusion zone ($X/\delta_{av} = 2.3$) and the fourth measurement location, 232mm from the slot, is approaching final zone behavior at ($X/\delta_{av} = 34.0$) although it is by definition in the transition zone. Plots of Y/λ vs C/C_{max} for these two locations are presented in Figures 6.5 and 6.6 for a $5Q_s$ injection rate. The scatter of the data points in Figure 6.6 is due to the low intensity of the fluorescence signal at the measurement location. The signal drop-off for the three pixels

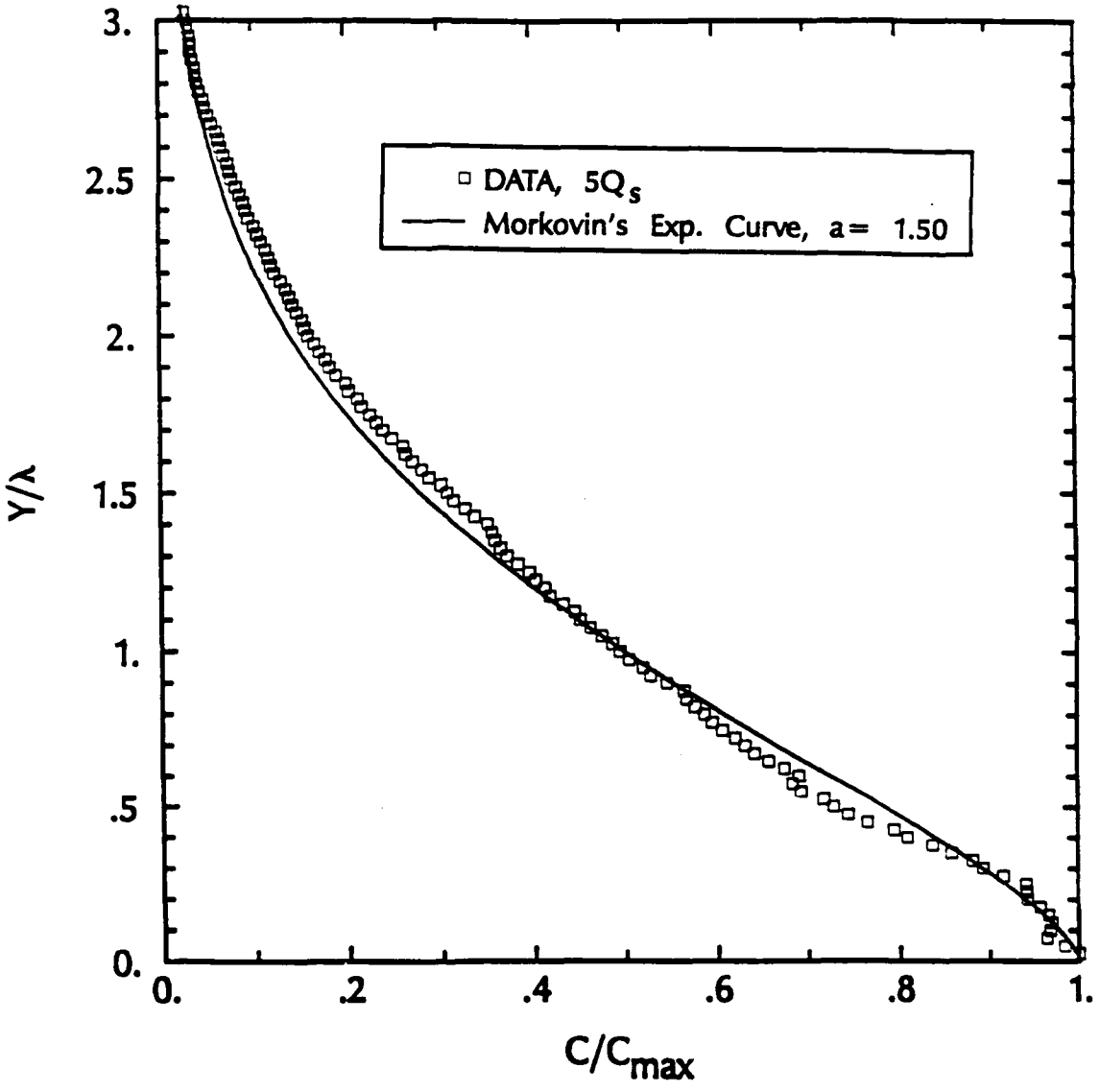

Figure 6.5. Plot of C/C_{max} vs Y/λ in the Intermediate Zone With Water Injection, $\bar{U}$= 4.6m/s, X= 12.7mm, X/δ_{av}= 2.3

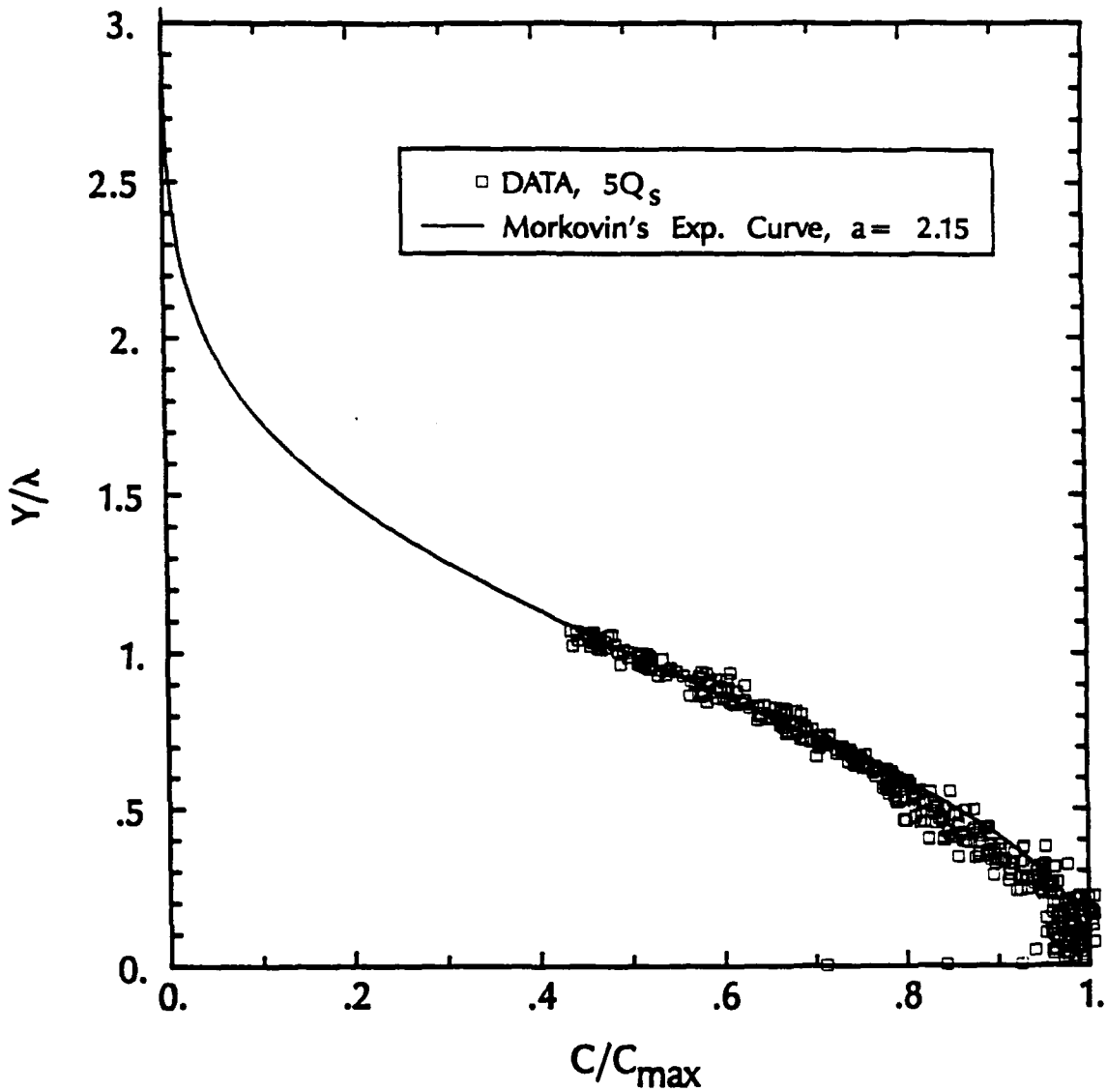

Figure 6.6. Plot of C/C_{max} vs Y/λ in the Transition Zone With Water Injection, $\bar{U}$= 4.6m/s, X= 232mm, X/δ_{av}= 34.0

nearest the wall in the same figure can be attributed to the combination of data scatter, vibration, and uncertainty as to the precise location of the wall on the array. The solid lines in both figures are the universal curves of Morkovin (1965), and again the agreement with the present results is excellent.

6.2 Polymer Injection Results

As with water, polymer was injected into the TBL at freestream velocities of 4.6 and 9.1m/s at rates from 2 to $10Q_s$. Mean polymer concentration profiles 12.7mm from the slot at both velocities are shown in Figures 6.7 and 6.8. Again, the maximum measured concentration is at the lowest freestream velocity and highest injection rate and is equal to the injection concentration within 1%. However, the measured polymer maximum concentration is at $Y^+ = 23$ (based on pure water scales), approximately, and drops 14% to the wall. The peak concentration for the other conditions plotted is also displaced away from the wall. This drop-off at the wall, however, is not believed to be real and is thought to result from index of refraction variations between water and the injectant. The size of the measured drop from the maximum value near the wall increases with polymer concentration, and the peak value moves away from the wall as the injection rate (i.e., and near wall concentration) is increased. The index of refraction of the polymer solutions is slightly higher than that of water. At 20

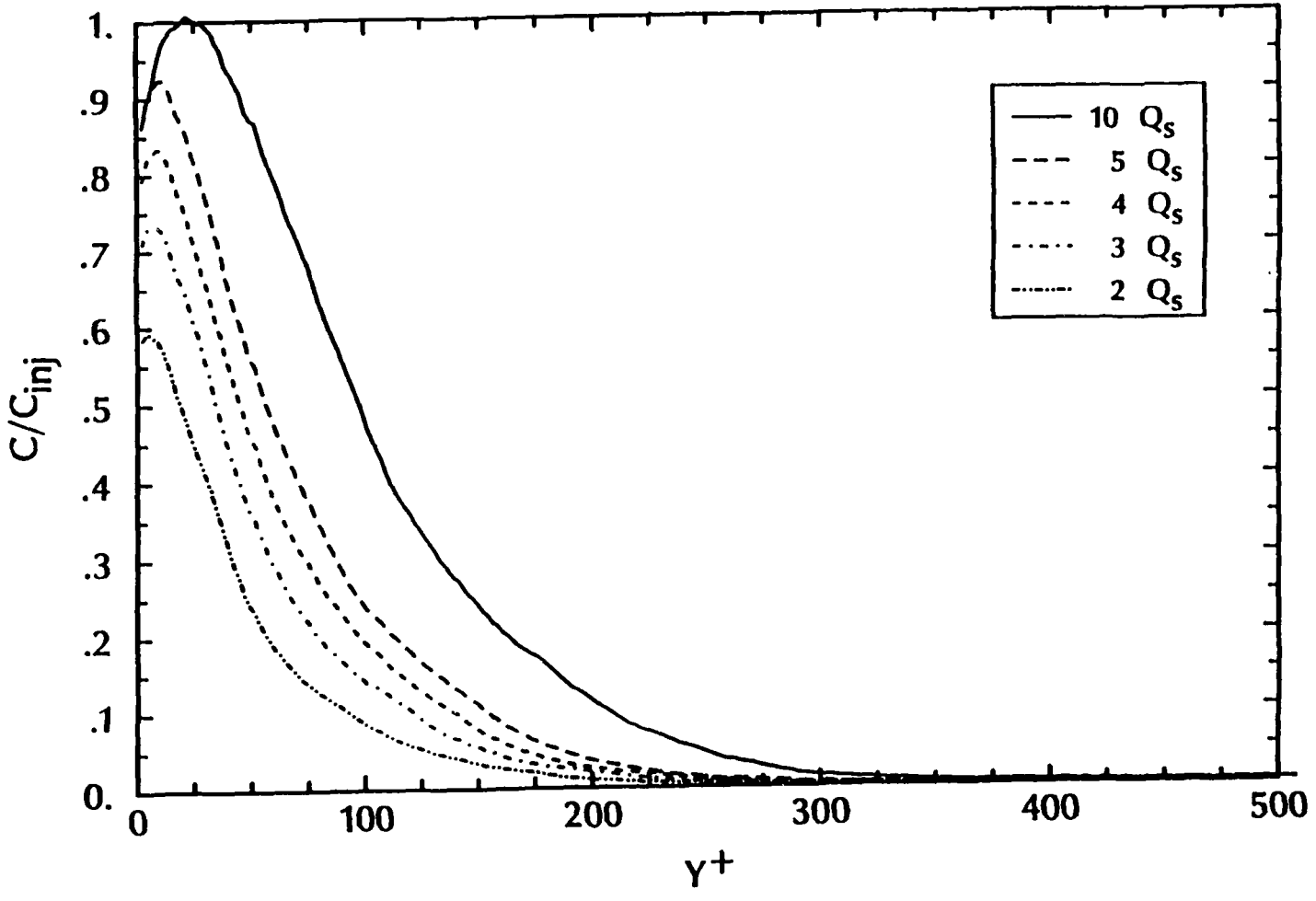

Figure 6.7. Polymer Mean Concentration Profiles at U= 4.6m/s, C_{inj}= 500wppm, X= 12.7mm, X/δ_{av}= 2.3

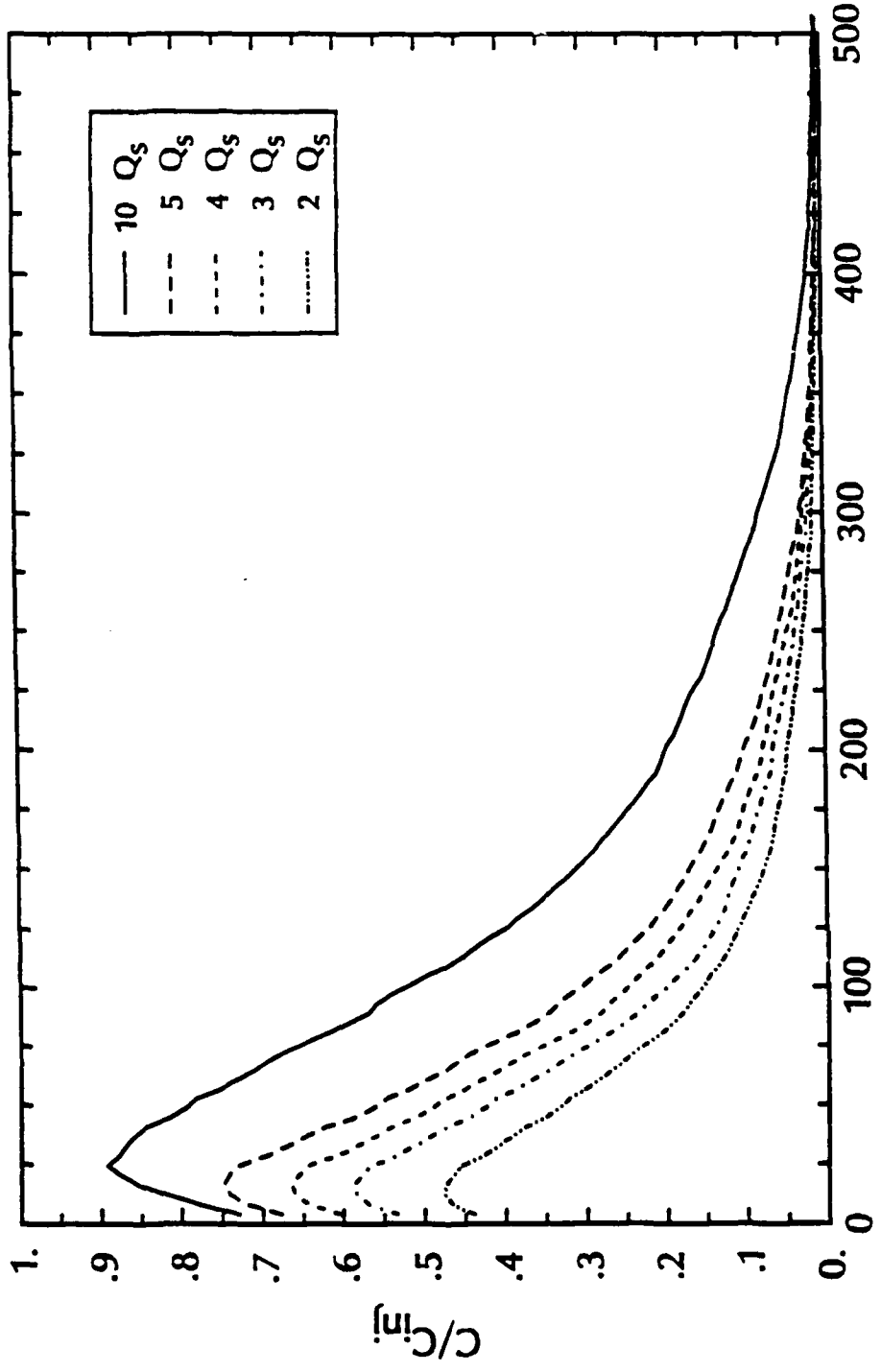

Figure 6.8. Polymer Mean Concentration Profiles at U= 9.1m/s, C_{inj}= 500wppm, X= 12.7mm, X/δ_{av}= 2.6

degrees Celsius, the measured indices of refraction for tap water, 500wppm polyethylene oxide and 1000wppm polyethylene oxide are 1.3306, 1.3308, and 1.3310 respectively. Although these seem like very small differences, ray tracing calculations indicate beam deflections due to the index gradient may be as large as 0.3 degrees. This optical aberration defocuses the signal very near the surface. The weak signals reflected off the surface are imaged partially by the near wall pixels, and the result is the observed drop off. The data taken at the most upstream location are most effected and is felt to establish the maximum possible error in the concentration at the wall at this injection concentration. Assuming that the maximum concentration is representative of the concentration at the wall should reduce the error associated with the signal drop-off and provide a reasonably accurate estimate.

For comparison to the water results in Figures 6.3 and 6.4, Figures 6.9 and 6.10 show the 500wppm polyox diffusion results at 4.6 and 9.1m/s respectively. The mass diffusion of the polymer is appreciably slower than that of the water initially. The polymer maintains a concentrated layer on the wall exhibiting what Poreh and Cermak (1964) define as initial zone behavior as far downstream as X/δ_{av}= 34.0 at 4.6m/s and X/δ_{av}= 20.7 at 9.1m/s. Unlike the water results in the intermediate and transitional diffusion zones in Figures 6.3 and 6.4 which exhibit no dependence on the injection rate, the polymer diffusion layer thickness increases with

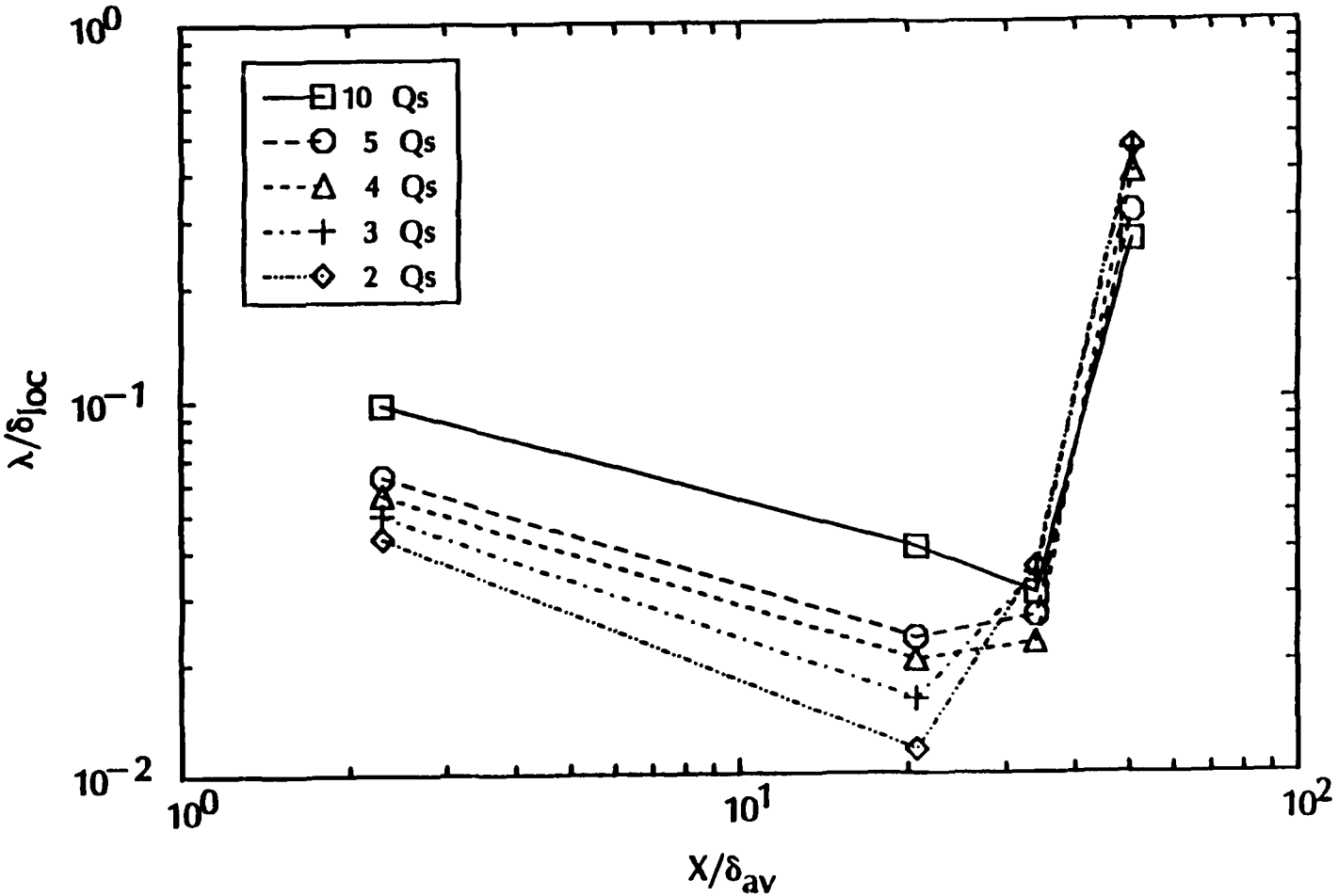

Figure 6.9. Diffusion to Viscous Boundary Layer Thickness Ratio Versus Streamwise Position With Polymer Injection, C_{inj}= 500wppm, U= 4.6m/s

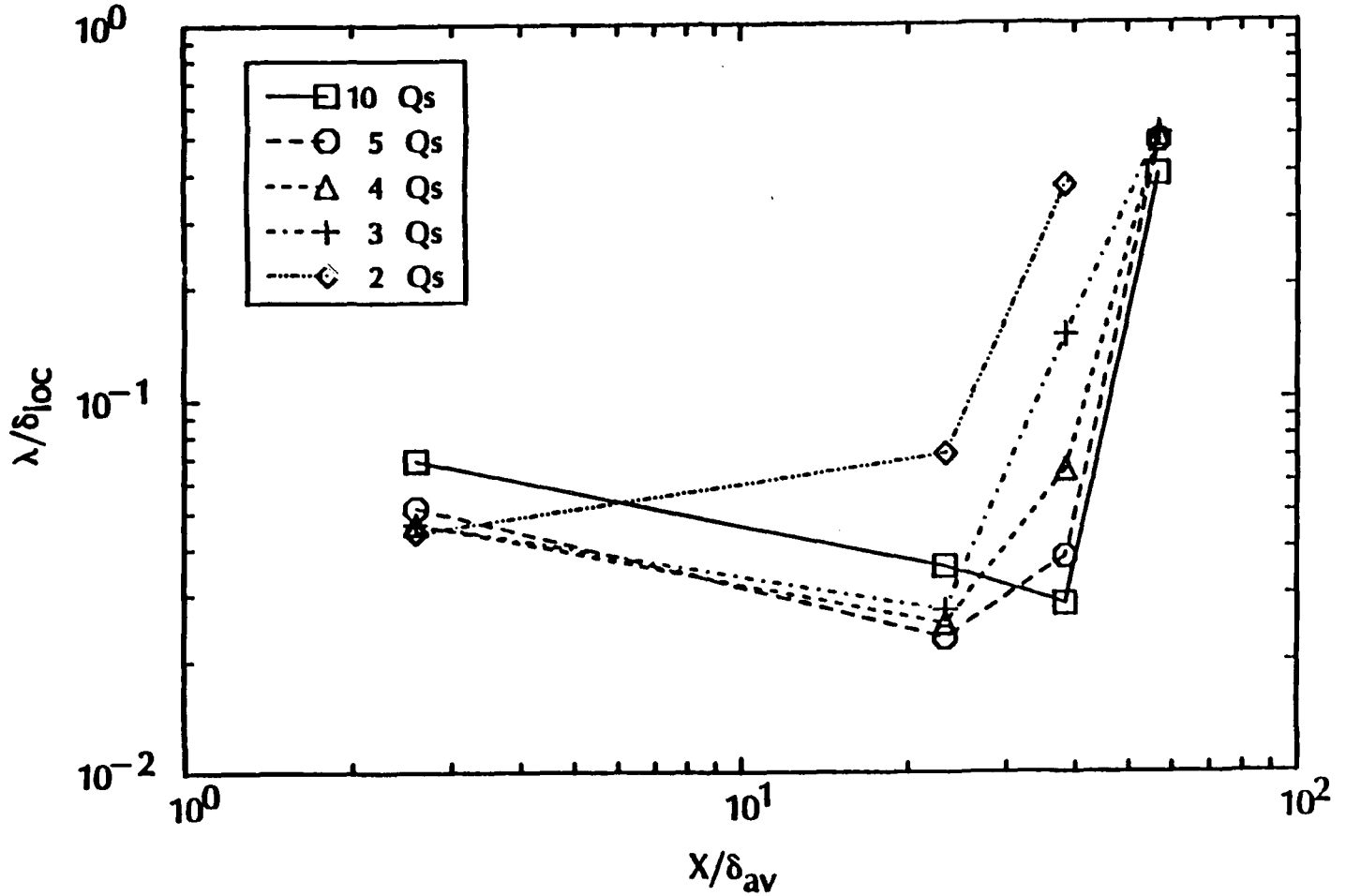

Figure 6.10. Diffusion to Viscous Boundary Layer Thickness Ratio Versus Streamwise Position With Polymer Injection, C_{inj}= 500wppm, U= 9.1m/s

injection rate in this region of initial zone behavior. The streamwise length of the initial zone also increases with the polymer injection rate. An abrupt increase in the diffusion layer thickness occurs at the end of the initial zone. This is consistent with previous studies [Latto and El Reidy (1976), Fruman and Tulan (1974)]. Since this rapid growth begins farther upstream at the lower injection rates, a trend reversal results and the lowest injection rate corresponds to the thickest diffusion layer. Of course, further downstream in the final zone no dependence of the diffusion layer thickness on the injection rate is possible. Only the concentration level or C_{max} will remain proportional to the injection rate.

Figure 6.11 is a plot of C/C_{max} vs Y/λ for 500 wppm polyox injection, 12.7mm from the slot, at a freestream velocity of 4.6m/s and a $5Q_s$ injection rate. With the exception of the $10Q_s$ injection rate at the same location and velocity, this test condition represents the maximum possible error in the measurement of C_{wall} due to index of refraction effects. Since the index of refraction problem is directly proportional to the local polymer concentration; and, for a given injection rate, the polymer concentration decreases with increasing streamwise distance, the error in measuring C_{wall} must decrease downstream. Assuming that the maximum concentration is representative of the concentration at the wall indicates that the measured wall concentration is

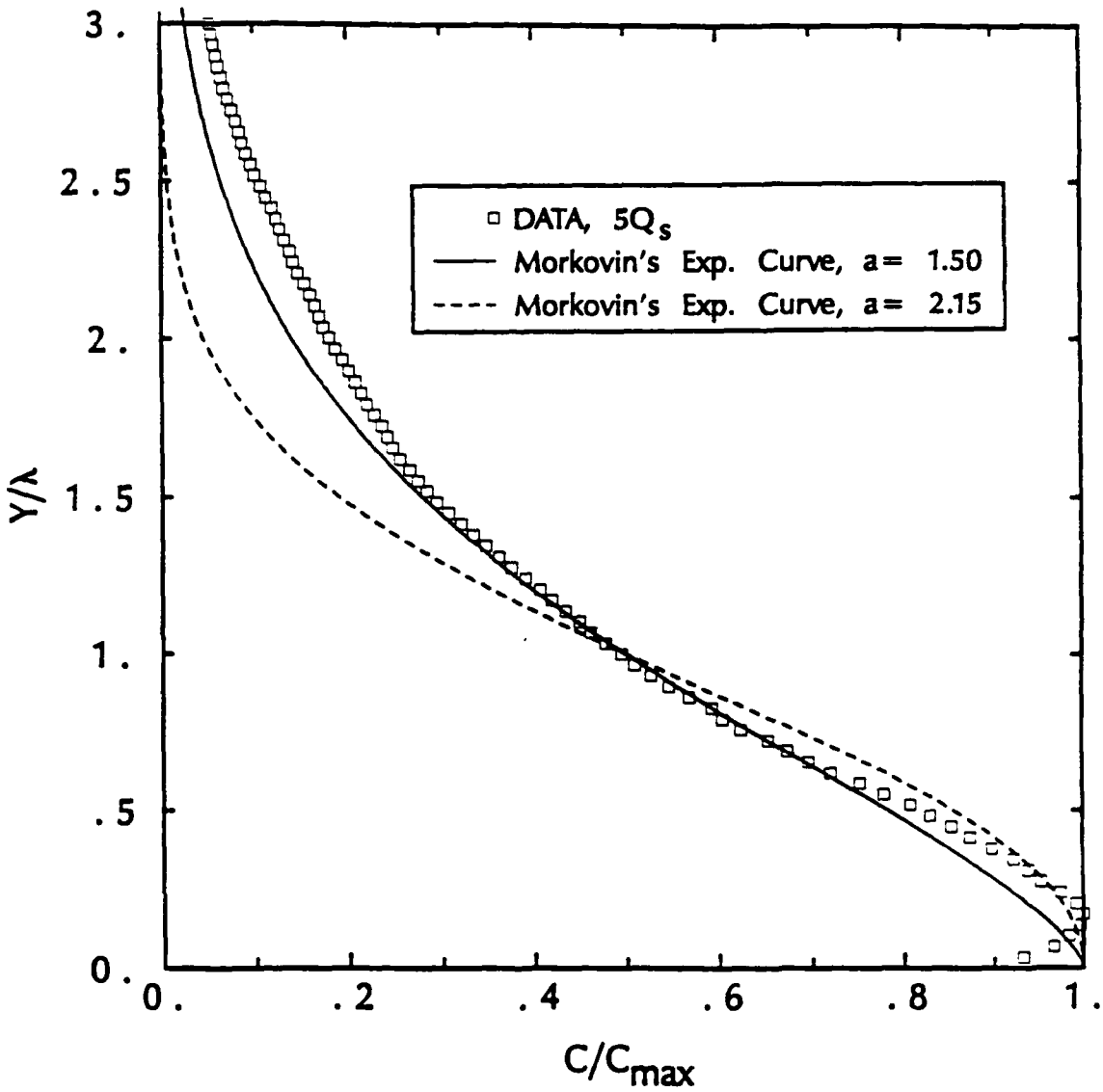

Figure 6.11. Plot of C/C_{max} vs Y/λ With Polymer Injection, C_{inj}= 500wppm, U= 4.6m/s, X= 12.7mm, X/δ_{av}= 2.3

approximately 7% low. This assumption seems reasonable since in Figure 6.7, the $10Q_s$ injection condition value of C_{max}/C_{inj}= 1.0 within 1% although it is displaced from the wall. Another reasonable approximation is that at heights not too far above the wall, the actual concentration profile is equal to the measured profile when shifted toward the wall by the distance necessary for C_{max} to equal C_{wall}. This should be valid since the fluorescence signal at a height Y above the surface is partially imaged by an array pixel at a height Y+ΔY where ΔY= Yc_{max}-Yc_{wall}. However, as the distance above the wall increases, and, therefore, the local polymer concentration decreases, this approximation becomes less accurate.

The data presented in Figure 6.11 come surprisingly close to fitting Morkovin's (1965) intermediate zone result (i.e., a= 1.5). The data are up to 5% high compared to Morkovin's curve, and a 5% shift of the concentration peak toward the wall would give agreement identical to that obtained with water up to Y/λ= 1.0. A 7% shift of the concentration peak toward the wall would result in a slightly larger near wall concentration gradient compared to Morkovin's curve. Above Y/λ= 1.0, values of C/C_{max} with polymer injection are higher than corresponding water injection values for both peak displacements. However, in any case, for a given injection rate and test velocity, the error associated with the measurement of C_{max}, C_{wall}, and the location of the concentration

peak due to index of refraction effects, must decrease downstream from where this measurement was performed.

For direct comparison to the dyed water injection results for the same test condition at the fourth measurement location, Figure 6.12 presents the corresponding polymer injection profile overlayed on Figure 6.6's water profile. The fields of view for both water injection and polymer injection were the same with the difference in span of Y/λ for the two curves in Figure 6.12 being due to the larger value of λ for the water injection case. Also, the excessive drop-off at the first pixel above the wall for the polymer injection curve in the same figure can again be attributed to vibration and uncertainty as to the precise location of the wall on the array.

At the fifth measurement location, 384mm from the slot, at a freestream velocity of 4.6m/s and a $5Q_s$ injection rate, the 500wppm polymer value of λ/δ_{loc} is 0.31. At these conditions, this location is, by passive contaminant definitions, in the intermediate diffusion zone. Figure 6.13 compares the polymer data to Morkovin's curve. Like the polymer data in Figure 6.12, the polymer data in Figure 6.13 is obviously not describable by the quasi-similarity relationships for a passive contaminant.

While the polymer profile in Figure 6.11 is close to the data obtained with water injection, the two plots of injected polymer C/C_{max} vs Y/λ, in Figures 6.12 and 6.13, bear little resemblence to

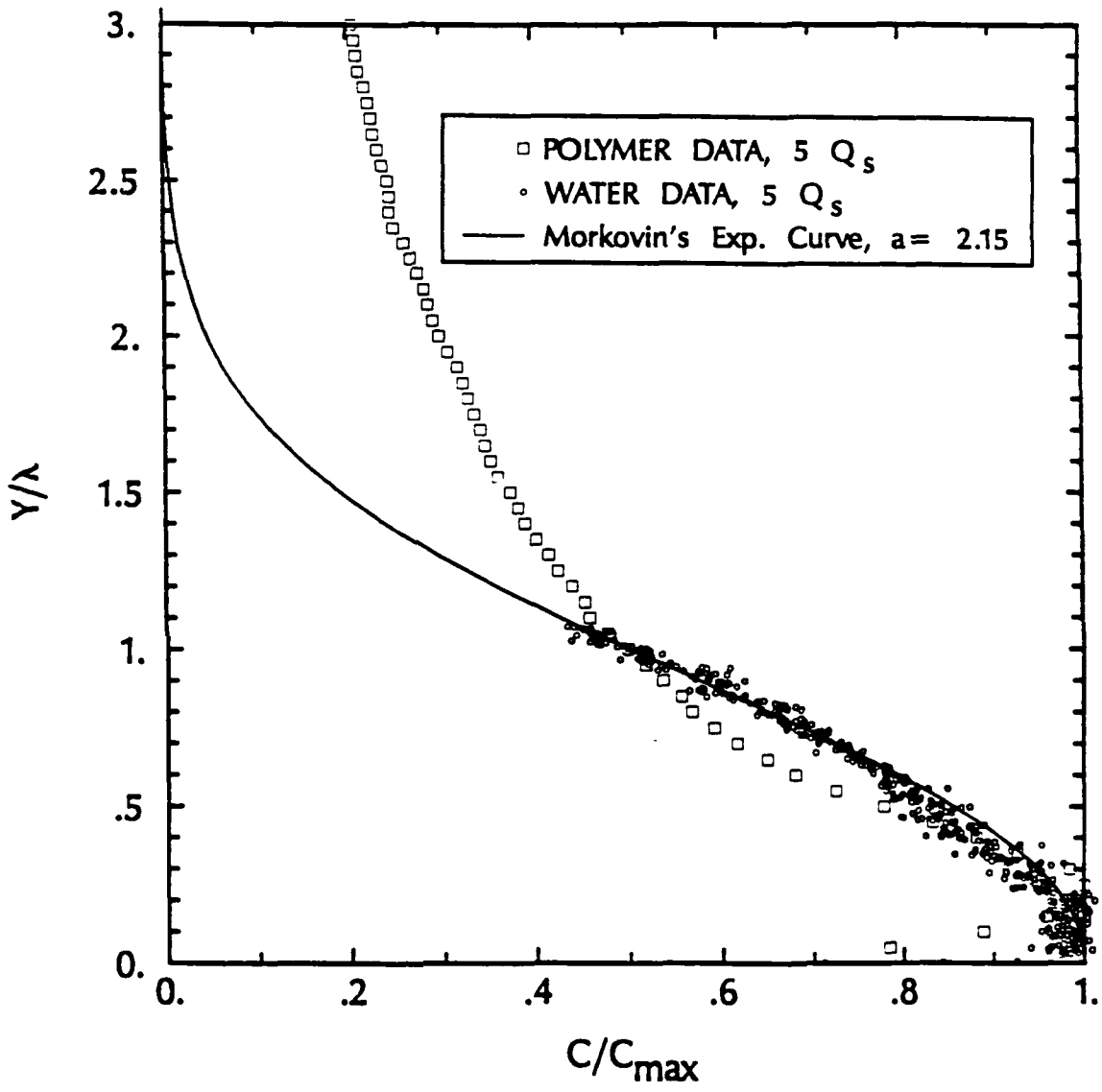

Figure 6.12. Plot of C/C_{max} vs Y/λ for Both Water and Polymer Injection at the Same Test Condition, C_{inj}= 500wppm, U= 4.6m/s, X= 232mm, X/δ_{avg}= 34.0

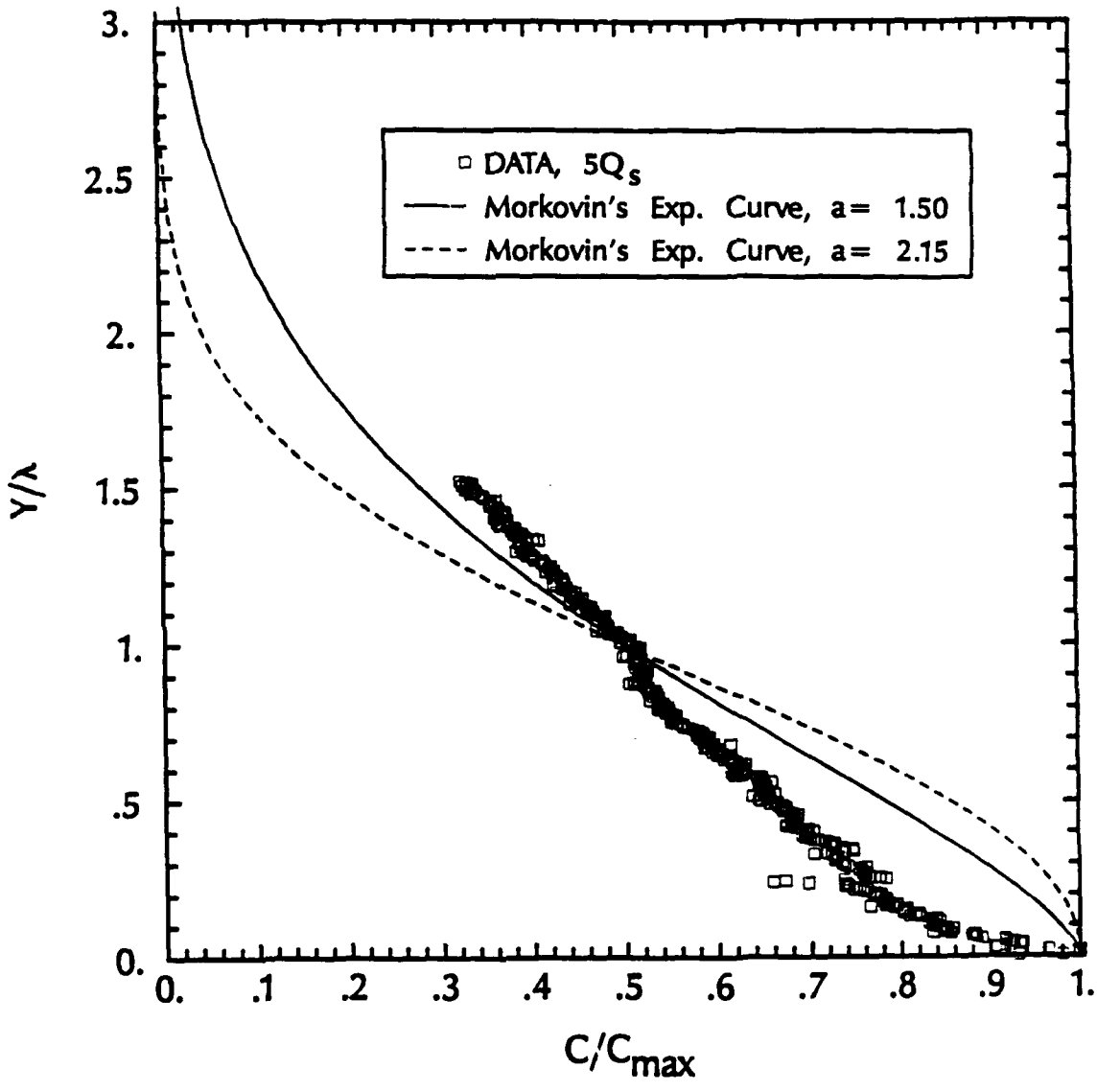

Figure 6.13. Plot of C/C_{max} vs Y/λ With Polymer Injection, C_{inj}= 500wppm, U= 4.6m/s, X= 384mm, X/δ_{av}= 50.5

the water results. Since the data for the latter two figures were taken downstream from the first measurement location, the error in the location of C_{max} should be less than approximately 7%. Both profiles show larger concentration gradients near the wall and larger values of C/C_{max} relative to water above $Y/\lambda = 1.0$. This was the case for all the profiles measured downstream from the first measurement location. In Figure 6.13, the data were taken at the fifth measurement location, and C_{max} is located at the wall. In Figure 6.12, the data were taken at the fourth measurement location, and the peak concentration is displaced away from the wall. However, a 5% shift of the concentration peak toward the wall would only make the plot of C/C_{max} vs Y/λ look more like the data in Figure 6.13. The big gap between data and Morkovin's curve in the outer part of the flow would still exist.

Wetzel and Ripken (1970) compared their final diffusion zone polymer results to Morkovin's (1965) empirical relation and obtained good agreement. In the current study, even at the fifth measurement location and 9.1m/s test velocity, the value of λ/δ_{loc} for polymer injection was slightly less than the $\lambda/\delta_{loc} = 0.64$ value characteristic of the final diffusion zone at all injection rates where extrapolation was not needed to determine λ. Thus, final zone behavior for polymer injection was not measured in this investigation. However, as final zone behavior is approached, there is a definite loss of the concave shape of the polymer

injection Y/λ vs. C/C_{max} curve which was so evident in Figures 6.12 and 6.13. Figure 6.14 is a plot of Y/λ vs C/C_{max} for 500wppm polyox injection, at the fifth measurement location, at a 9.1m/s test velocity and $5Q_s$ injection rate. Compared to the profiles measure upstream, and to the profiles measured at this location at lower test velocities and/or higher injection rates, this profile is shifted toward Morkovin's exponential curves. Indeed, above $Y/\lambda = 0.5$, the polymer curve presented in Figure 6.14 almost overlaps Morkovin's ($a = 1.5$) intermediate zone result.

At the same test condition but lower injection rates, λ was located farther from the surface than the array could measure. Extrapolating the data for the 4 and $3Q_s$ injection rate conditions resulted in C/C_{max} vs Y/λ profiles very similar to that obtained in Figure 6.14. For the $2Q_s$ injection condition, λ was located too far from the surface to have confidence in the extrapolated result.

In addition to their final diffusion zone measurements, Wetzel and Ripken (1970) presented a plot of Y/λ vs C/C_{max} for injection of very concentrated solutions of polyox measured downstream where final zone mixing is not quite achieved. These data bear strong resemblence to the polymer profiles presented in Figures 6.12 and 6.13 in the current study. Wetzel and Ripken's data show slightly larger near wall concentration gradients and larger values of C/C_{max} relative to Morkovin's ($a = 2.15$) curve above $Y/\lambda = 1.0$. However, since the concentration profile measurements were performed with

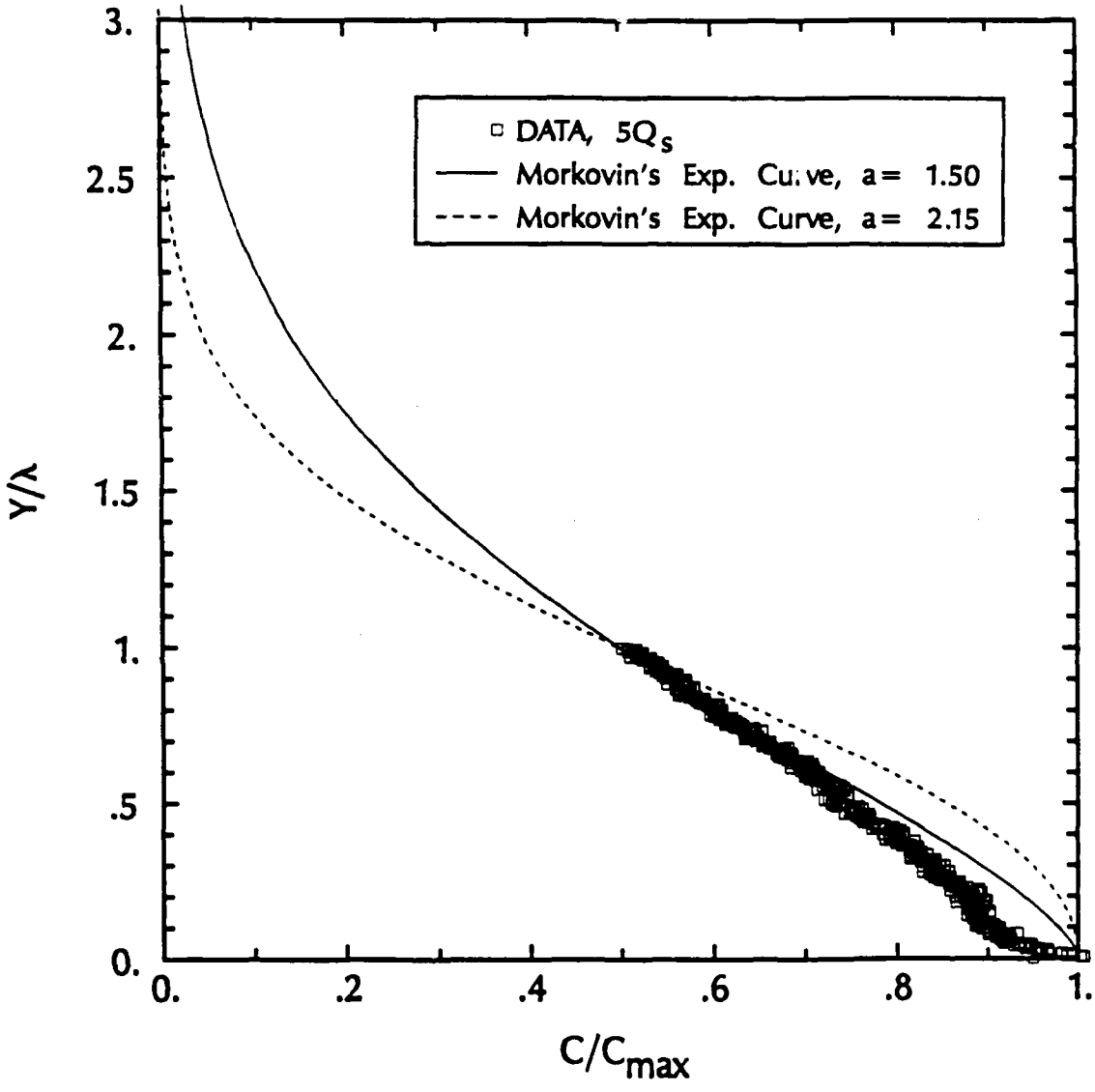

Figure 6.14. Plot of C/C_{max} vs Y/λ With Polymer Injection, C_{inj}= 500wppm, U= 9.1m/s, X= 384mm, X/δ_{av}= 56.7

conventional probe sampling techniques, the measured value of C_{max} is probably low due to the probe's inability to resolve the true concentration very near the wall where the concentration gradient is largest. The effect of a low measured value of C_{max} would be to overpredict λ. Thus, a higher value of C_{max} and a lower value of λ would result in a profile even more similar to the data presented in Figures 6.12 and 6.13.

In addition to mean concentration profiles, one may gain further insight into the diffusion process by examining higher order central moments of the near instantaneous data. While any contaminating noise in the instantaneous concentration measurements will introduce error into the data statistics, the signal to noise ratio in the current study is sufficiently high to minimize these effects. The noise present when performing the concentration measurements is, as discussed in Chapter 4, approximately Gaussian with a standard deviation ranging from 6.5 to 10% of the mean concentration value. This contaminating noise will have no effect on the mean concentration, will tend to increase the standard deviation, and will slightly weight the skewness and kurtosis toward Gaussian values.

Figure 6.15 shows the standard deviations of the polymer concentration fluctuations, C', under the same conditions as in Figure 6.7, where

$$C'^2 = \frac{\sum_{k=1}^{N} (C_k - C_A)^2}{N} \quad . \tag{6.2}$$

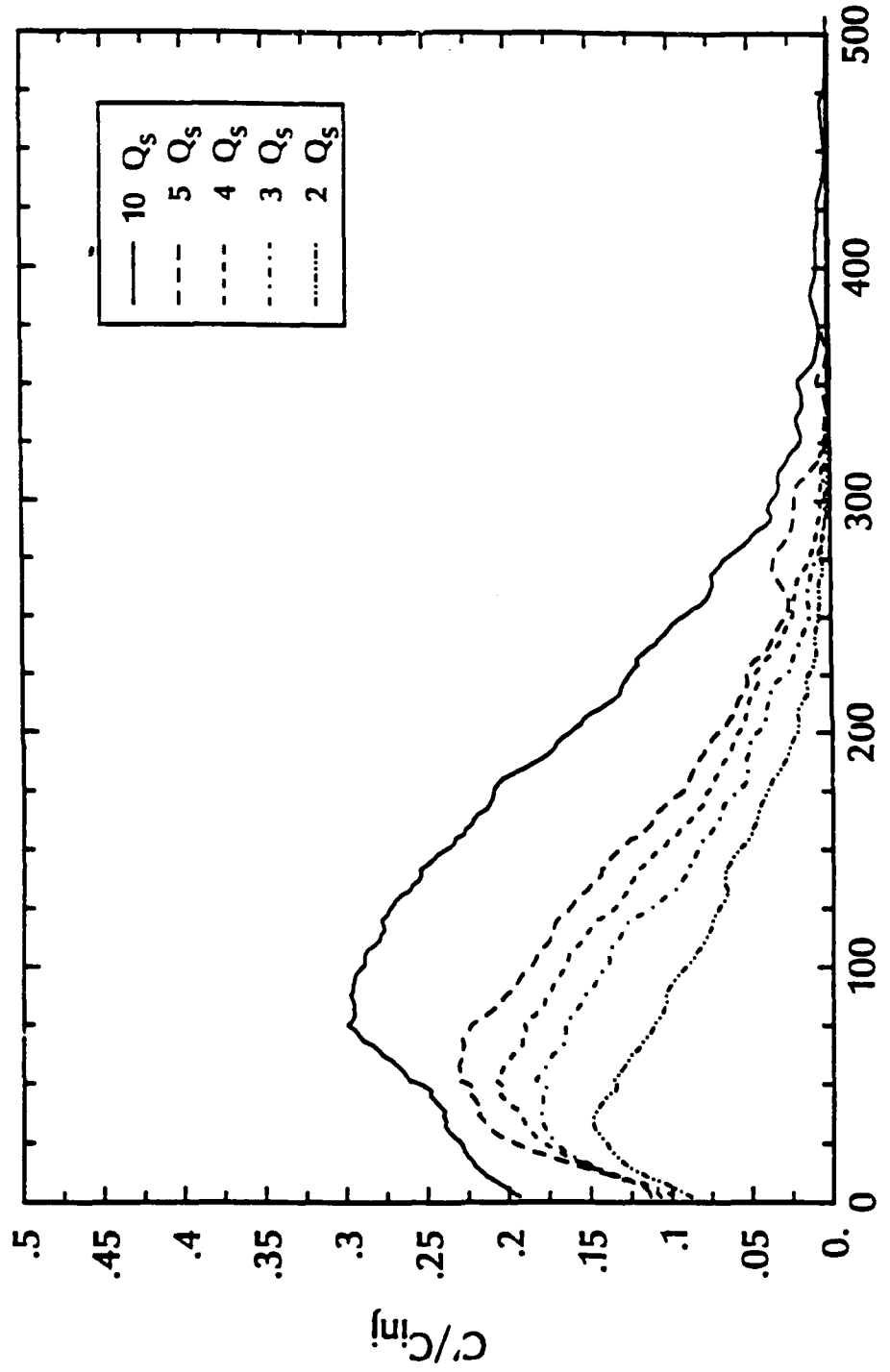

Figure 6.15. Polymer Concentration Standard Deviation Profiles at U= 4.6m/s, C_{inj}= 500wppm, X= 12.7mm, X/δ_{av}= 2.3

The standard deviation has a peak above the wall that diminishes and moves toward the wall with decreasing injection rate, increasing free stream velocity, and increasing streamwise distance. A part of this decrease near the wall is a result of the decrease seen in the mean concentration profiles due to index of refraction effects. However, the dyed water standard deviation data shown in Figure 6.16 have similar maxima indicating that these polymer maxima are real. The observed polymer standard deviation maxima are displaced further from the wall and are much larger in relative magnitude than the mean concentration signal decrease. Figure 6.15 shows the concentration standard deviation to be almost zero above $Y^+ = 300$. This is consistent with the mean concentration profile in Figure 6.7 where above $Y^+ = 300$, C/C_{inj} is almost zero. Compared to the dyed water standard deviations in Figure 6.16, the polymer standard deviations are larger in magnitude below $Y^+ = 200$. Above $Y^+ = 200$, the concentration standard deviations of the polymer and the water appear almost identical. Again, this is consistent with the mean concentration profiles.

Figures 6.17 and 6.18 show distributions of skewness, Sk, and flatness factors, K, for the polymer concentration with the factors defined as follows:

$$Sk_i = \frac{\sum_{k=1}^{N} (C_k - C_A)^3}{NxC'^3} \qquad (6.3)$$

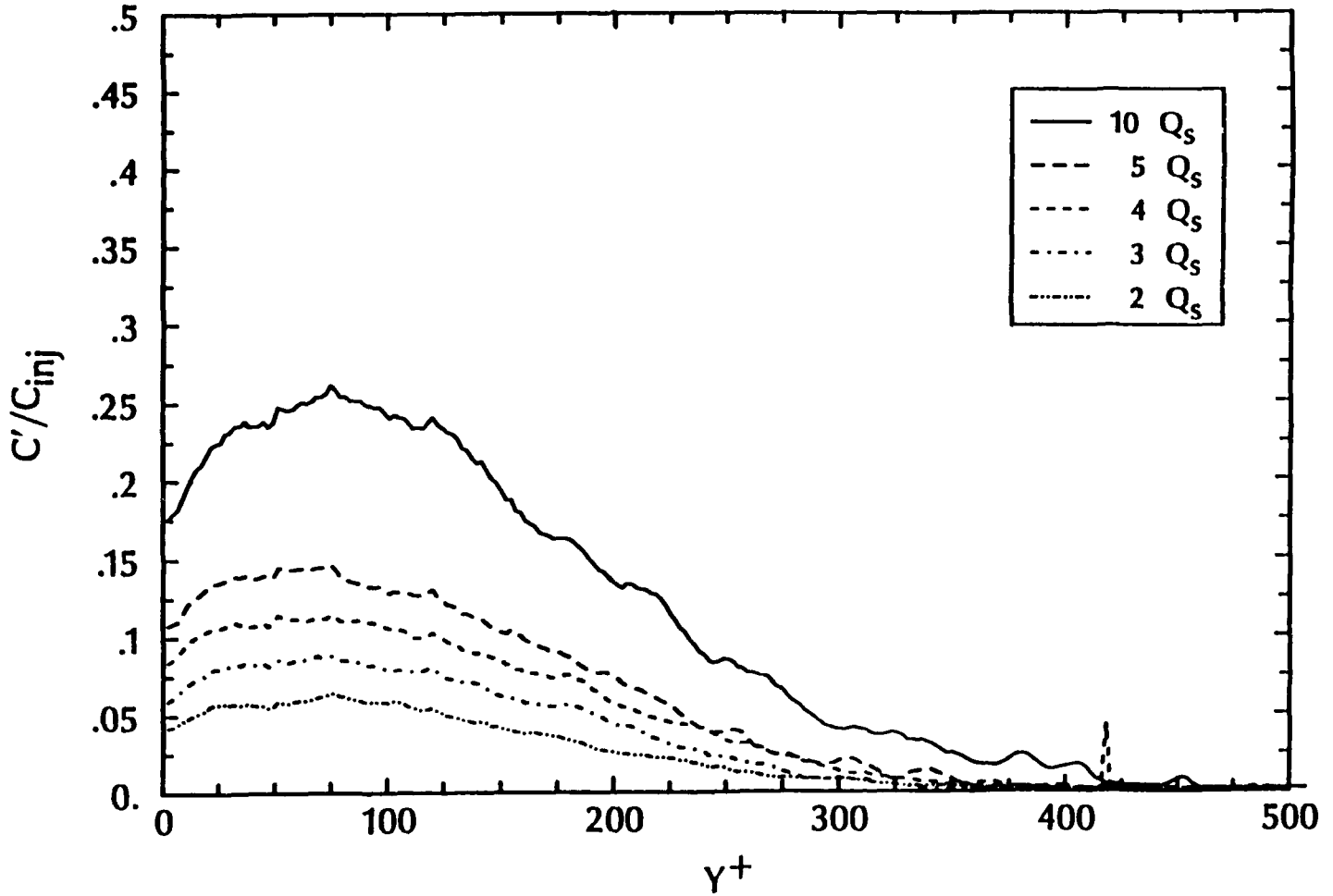

Figure 6.16. Dyed Water Concentration Standard Deviation Profiles at U= 4.6m/s, X= 12.7mm, X/δ_{av}= 2.3

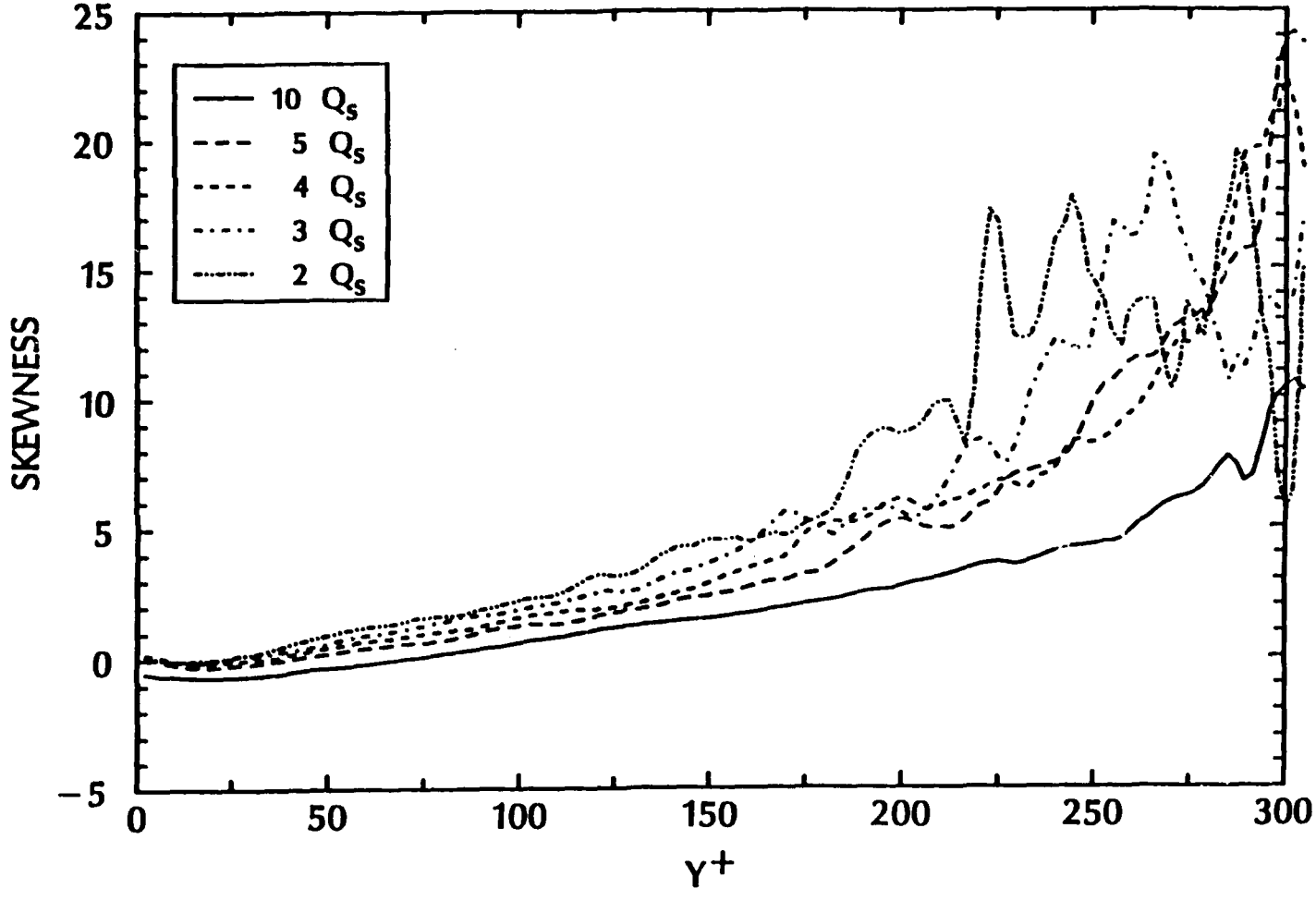

Figure 6.17. Polymer Concentration Skewness Factor Profiles at U= 4.6m/s, C_{inj}= 500wppm, X= 12.7mm, X/δ_{av}= 2.3

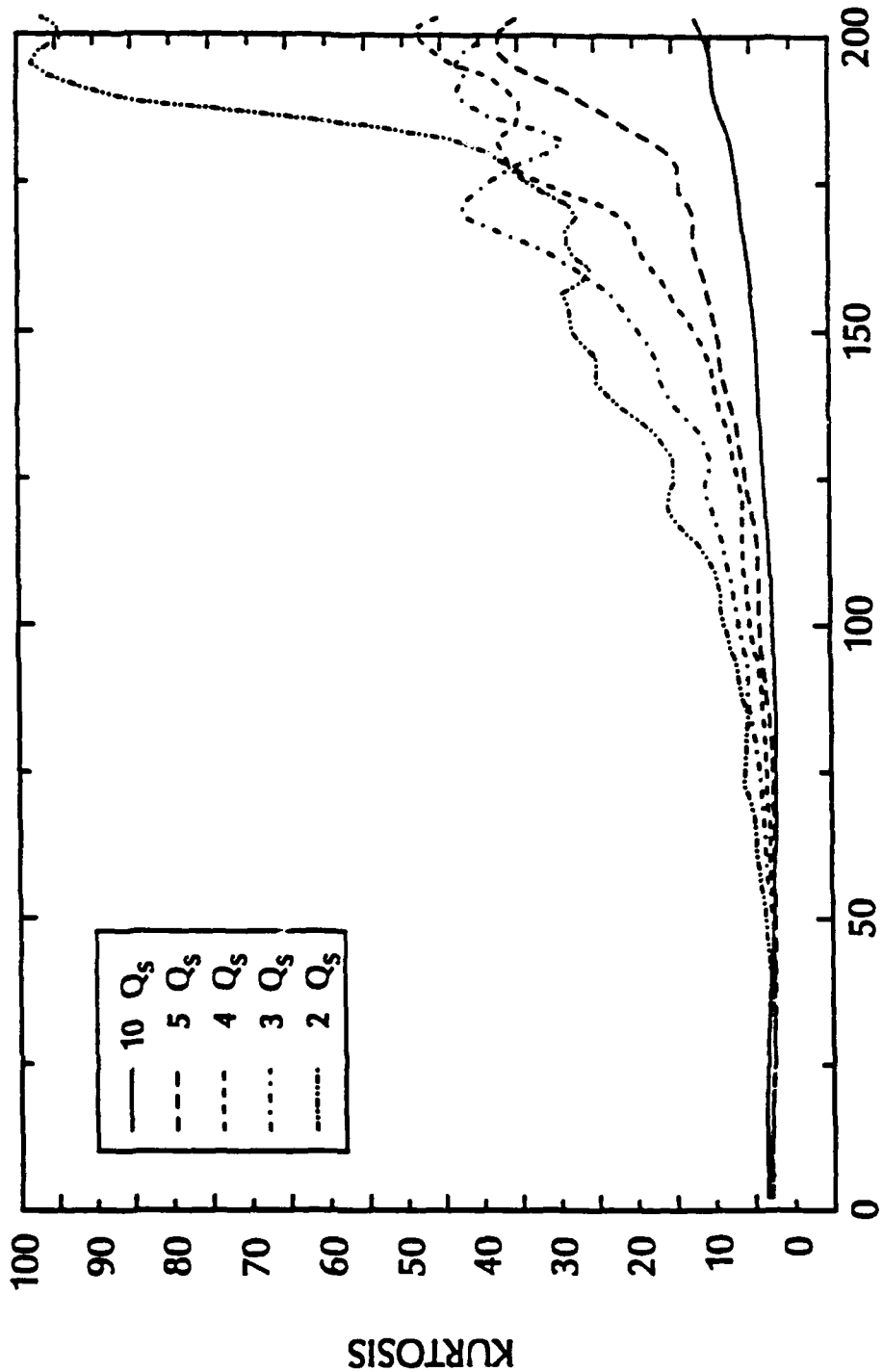

Figure 6.18. Polymer Concentration Flatness Factor Profiles at U= 4.6m/s, C_{inj}= 500wppm, X= 12.7mm, X/δ_{av}= 2.3

$$K_i = \frac{\sum_{k=1}^{N} (C_k - C_A)^4}{NxC'^4} \qquad (6.4)$$

The skewness factors exhibit an increase beginning at the wall from a nearly Gaussian value of 0 to a significantly positive value near 1.0 over a distance comparable to the 50% thickness, λ, and increase almost linearly until $Y^+ = 200$. The flatness factors increase monotonically from Gaussian values near the wall but the increase is not linear. Like the skewness factors, the flatness factors become highly irregular above approximately $Y^+ = 200$. This is due to the diminishing size of the standard deviation which is the normalization parameter for these factors and is due to statistical uncertainty.

The polymer skewness and flatness factor profiles in Figures 6.17 and 6.18 respectively are greater in magnitude than their corresponding water injection profiles in Figures 6.19 and 6.20. However, unlike the standard deviation profiles, the difference in magnitude increases with distance from the wall. These statistics indicate that the polymer lifts off the wall in more concentrated structures and in a more intermittent manner than does the water. Higher concentration polymer is occasionally observed farther from the wall whereas only dilute dyed water is present. Also, near the injection slot the polymer third and fourth order central moments exhibit an injection rate dependence

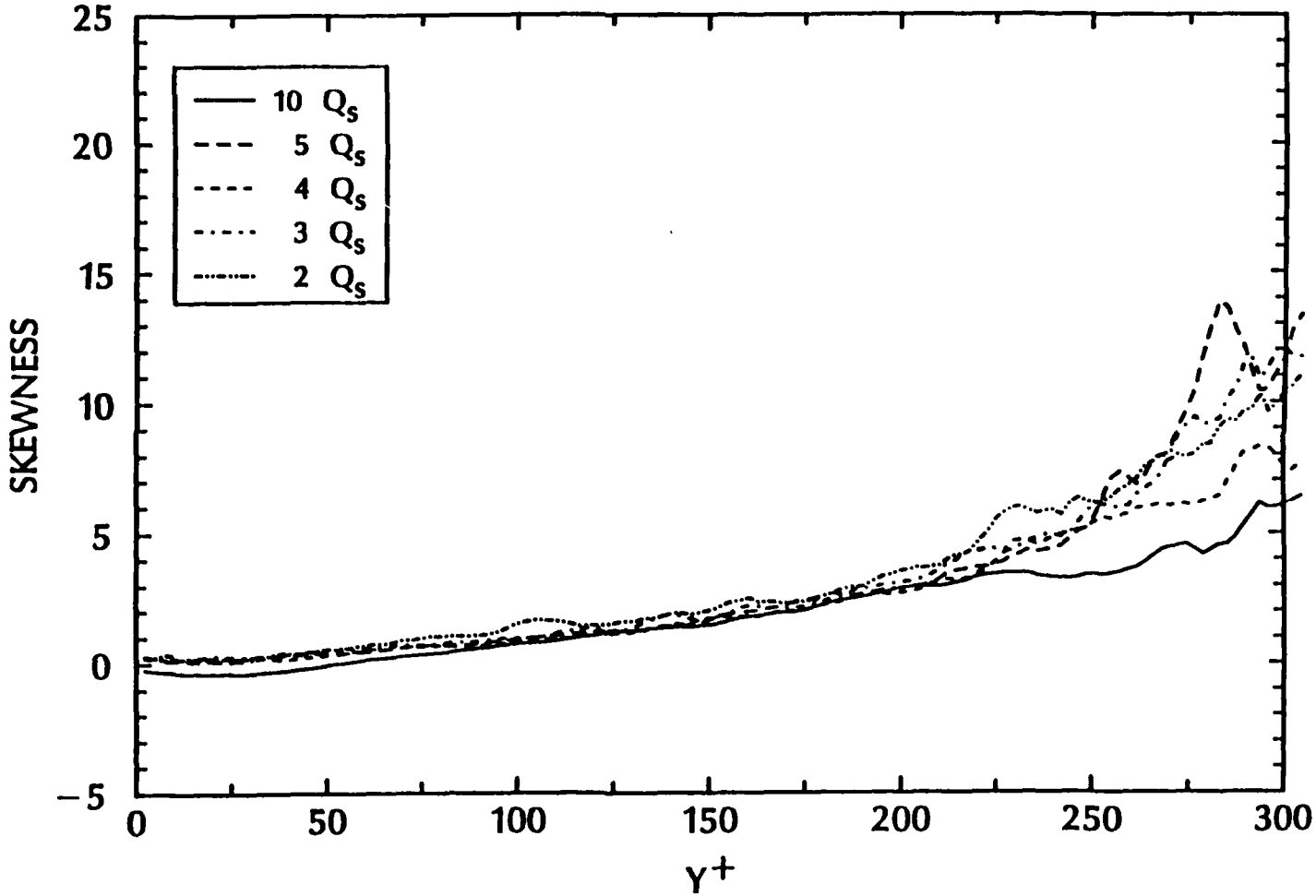

Figure 6.19. Dyed Water Concentration Skewness Factor Profiles at U= 4.6m/s, X= 12.7mm, X/δ_{av}= 2.3

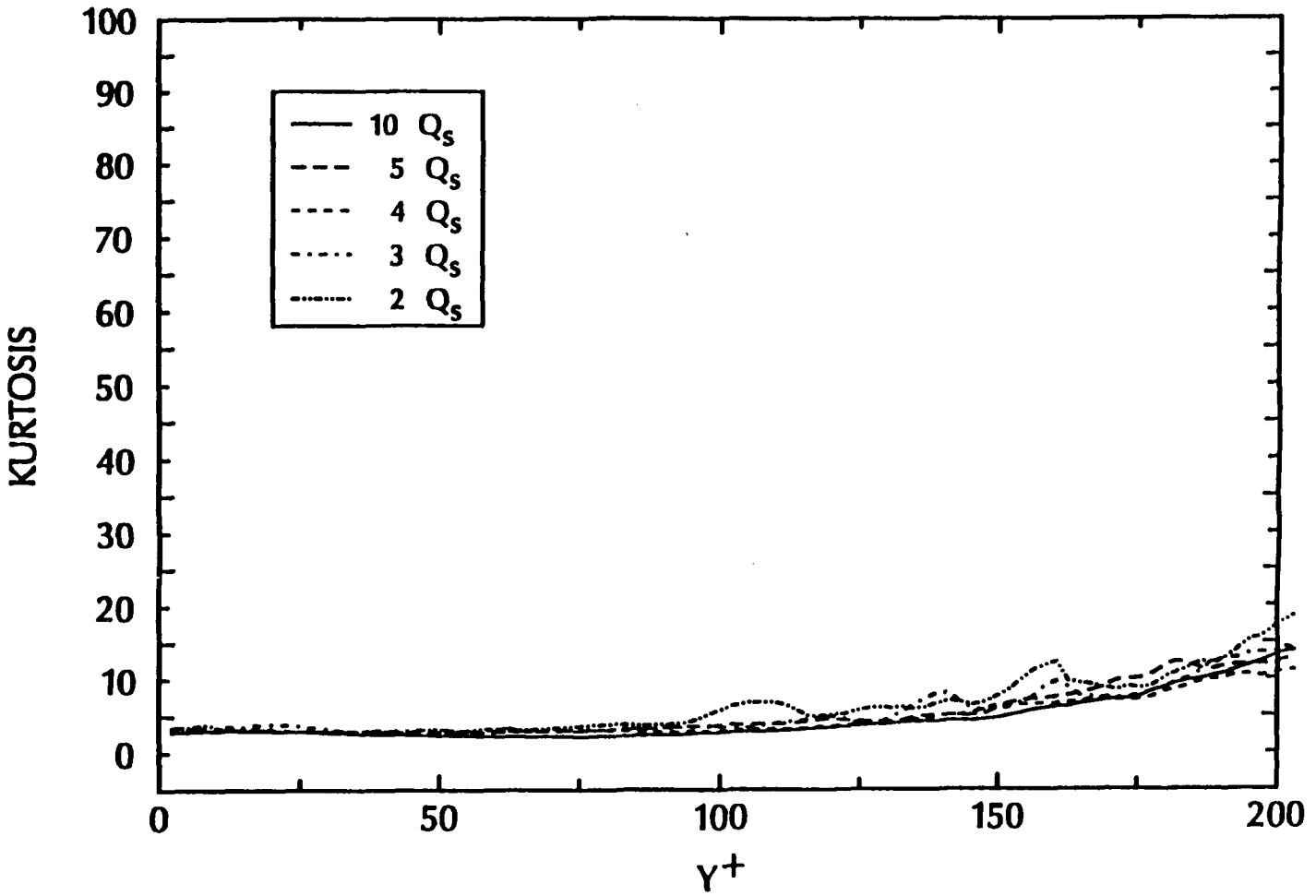

Figure 6.20. Dyed Water Concentration Flatness Factor Profiles at U= 4.6m/s, X= 12.7mm, X/δ_{av}= 2.3

not found with water. This injection rate dependence, however, disappears downstream as the polymer is diffused.

Another interesting analysis which may be performed on the near instantaneous concentration profile data is the computation of probability density functions (PDF's) of concentration as a function of distance from the wall. While PDF's contain no more information than the statistics discussed above, it is often easier to visualize the characteristics of the data record with them. Figures 6.21 through 6.24 show the PDF's of polymer injected at $5Q_s$ into the TBL with a freestream velocity of 4.6m/s, 12.7mm downstream of the slot. There are 35 bins along the abscissa in each PDF plot with the bin width being $\Delta C/C_{inj}$= 0.04 and the mean value of C/C_{inj} is denoted by a solid vertical line. The vertical measurement locations are Y^+= 10.7, 21.4, 53.6, 107, 161, 214, 428, and 643 based on pure water scales. As the polymer PDF's and mean concentration profile and statistics indicate, polymer concentrations approaching the injection concentration are found only near the wall. The mean concentration drops rapidly with increasing distance from the wall and the distributions become increasingly skewed positive. It should be mentioned here that, as shown in the PDF's near the wall, the Gaussian noise discussed in Chapter 5 causes some values of the instantaneous concentration to be recorded as greater than the injection concentration.

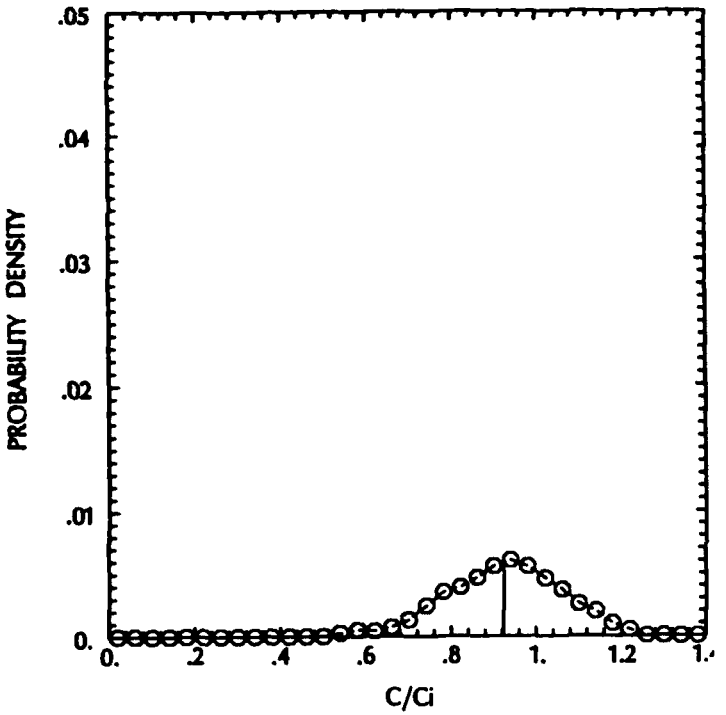

Y^+= 10.7

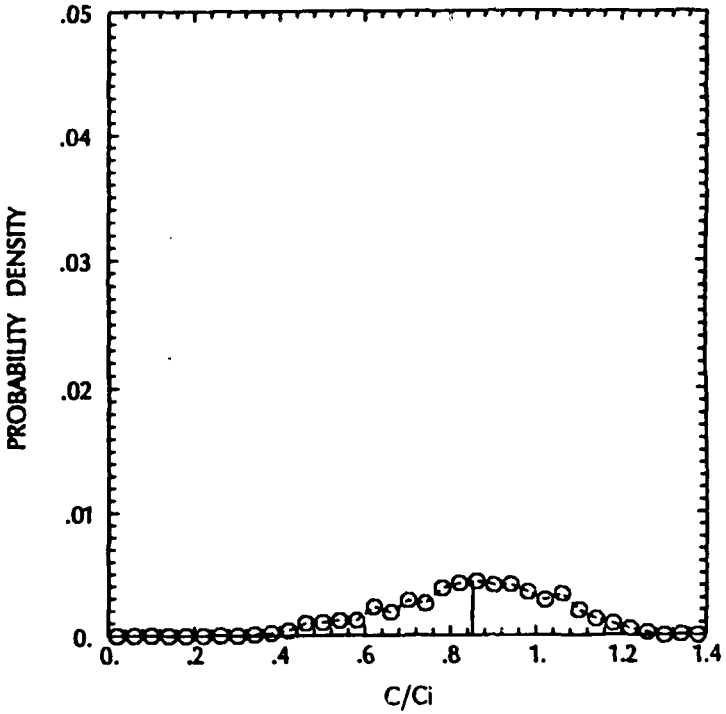

Y^+= 21.4

Figure 6.21. Polymer Concentration PDF at Y^+= 10.7 and 21.4, C_{inj}= 500wppm, U= 4.6m/s, X= 12.7mm, X/δ_{av}= 2.3

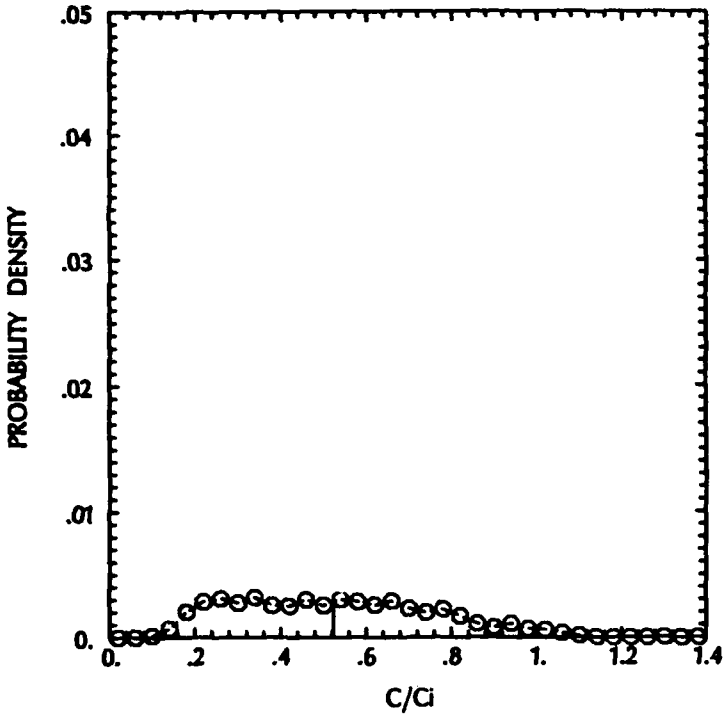

Y^+= 53.6

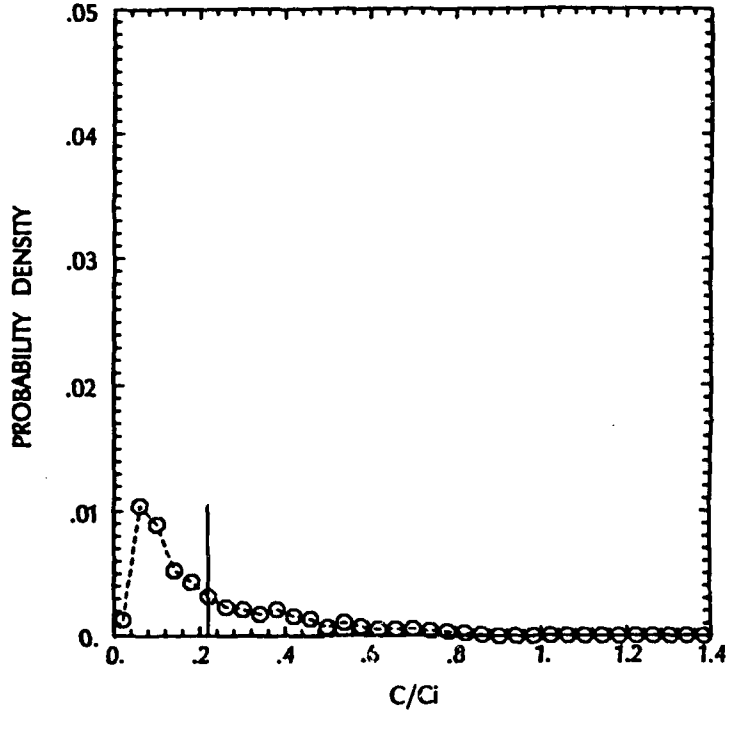

Y^+= 107.1

Figure 6.22. Polymer Concentration PDF at Y^+= 53.6 and 107, C_{inj}= 500wppm, U= 4.6m/s, X= 12.7mm, X/δ_{av}= 2.3

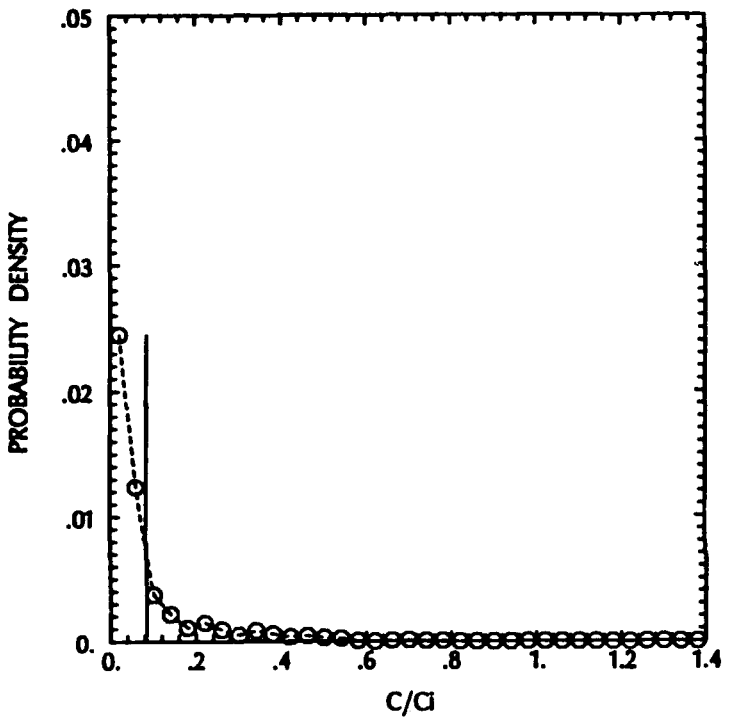

Y^+= 160.7

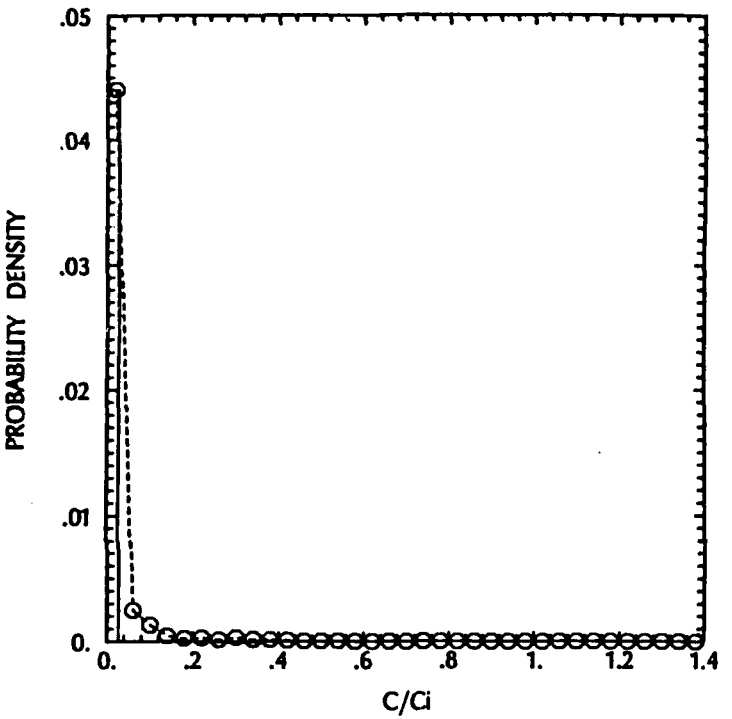

Y^+= 214.2

Figure 6.23. Polymer Concentration PDF at Y^+= 161 and 214, C_{inj}= 500wppm, U= 4.6m/s, X= 12.7mm, X/δ_{av}= 2.3

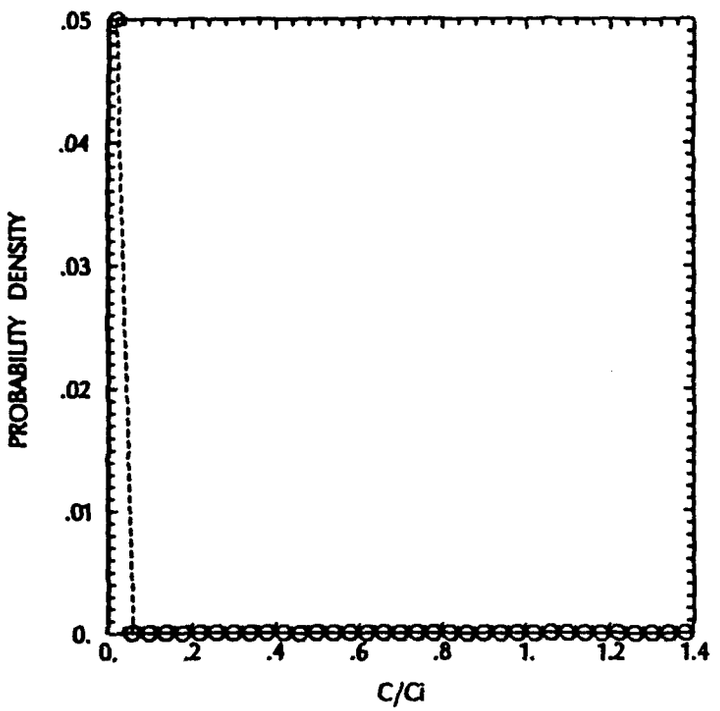

Y^+= 428.4

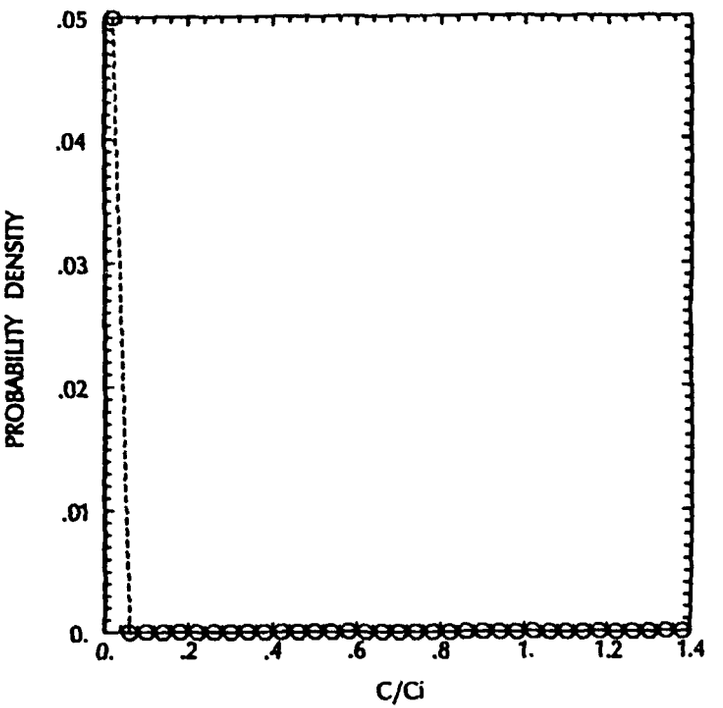

Y^+= 642.6

Figure 6.24. Polymer Concentration PDF at Y^+= 428 and 643, C_{inj}= 500wppm, U= 4.6m/s, X= 12.7mm, X/δ_{av}= 2.3

CHAPTER 7

SUMMARY AND RECOMMENDATIONS FOR FURTHER STUDY

7.1 Summary

A high resolution LIF technique for measuring near instantaneous concentration profiles of a fluid injected into a high unit Reynolds number turbulent boundary layer has been presented. The technique was used to measure water and polymer concentration profiles with a spatial and temporal resolution of 35 microns and 7.17 microseconds, respectively, at approximately 2.20x microscope magnification. At 5x magnification, the spatial resolution of the instrumentation exceeded 15 microns, although these data were not shown. The resolution of the LIF technique is limited, however, by the Kolmogorov length microscales of the subject flow. At spatial scales smaller than the Kolmogorov microscales, where molecular diffusion is dominant, the diffusion of the injectant is not precisely represented by the diffusion of the dye. This is due to the different molecular diffusivities of the dye and the injectant into water.

Results from a few of the many analysis which may be performed on the measured near instantaneous profiles were presented including plots of the mean, higher order central moments and concentration probability density functions as a function of distance from the wall. The passive contaminant line source

diffusion results of Poreh and Cermak (1964) have been duplicated using this technique. Mean polymer concentration profile data, which were in agreement with previous studies, were also acquired and presented. This LIF technique is a very powerful non-intrusive tool capable of achieving a level of resolution and a dynamic visualization not possible with previous, more conventional techniques.

7.2 Recommendations for Further Study

In using this LIF technique for concentration profile measurements, index of refraction variations between the tunnel water and the injectant lead to the observed signal drop-off very near the wall discussed in section 6.2. One obvious way of avoiding this drop-off would be to match the indices of refraction by heating or cooling either the water or the injectant. However, depending on the magnitude of the temperature difference between the fluids, the result may be to modify the actual diffusion process by introducing unknown buoyancy and density stratification effects. Modifying the subject diffusion process is clearly unacceptable with the only alternative being to somehow correct for the index of refraction effects.

A possible correction for this near wall signal drop-off in the mean is the development of corrections based on ray tracing and the measured mean concentration profiles. By assuming that the

mean maximum local injectant concentration is at the wall it should be possible to back out the very near wall concentration profile responsible for the displaced peak. This, however, is a complicated problem and the results are not easily verifiable. Simply resetting the wall to the injectant concentration peak without any computations should yield satisfactory near wall results. Attempting to correct the instantaneous profiles would be fruitless since the diffusion process is not only unsteady but three dimensional as well. The path which a light ray would travel on its way from the dye fluorescing in the laser beam to the microscope would depend on the instantaneous spanwise injectant concentration, which is unknown. Further investigations are necessary to find an acceptable solution to this problem.

REFERENCES

Falco, R. E. and Wiggert, D. C., "Effects of Dilute Polymer Solutions on Vortex Ring/Wall Interactions - A Mechanism for Drag Reduction," Viscous Flow Drag Reduction, edited by M. Summerfield for AIAA Progress in Astronautics and Aeronautics Series, V72, pp. 275-289, 1979.

Fruman, D.H. and Tulin, M.P., "Diffusion of a Tangential Drag Reducing Polymer Injection of a Flat Plate at High Reynolds Numbers," Journal of Ship Research, Vol. 20, No. 3, pp. 171-180, September 1976.

Gadd, G. E., "Effects of Drag Reducing Additives on Vortex Stretching," Nature, V217, pp. 1040-1042, March 1968.

Guilbualt, G. G., Practical Fluorescence, Marcel Dekker, Inc., New York, 1973.

Ippen, E. P., Shank, C. V., and Dienes, A., "Rapid Photobleaching of Organic Laser Dyes in Continuously Operated Devices," IEEE Journal of Quantum Electronics, QE-7, pp. 178-179, April 1971.

Koochesfahani, M. M., Experiments of Turbulent Mixing and Chemical Reactions in a Liquid Mixing Layer, Ph.D. thesis, California Institute of Technology, 1984.

Koochesfahani, M. M. and Dimotakis, P. E., "Laser-Induced Fluorescence Measurements of Mixed Fluid Concentration in a Liquid Plane Shear Layer," AIAA Journal, Vol. 23, No. 11, pp. 1700-1707, November 1985.

Lacey, P., "Drag Reduction by Long Chain Polymers," Chem. Eng. Sci., V29, pp. 1495-1496, 1974.

Latto, B. and El Riedy, O. K. F., "Diffusion of Polymer Additives in a Developing Turbulent Boundary Layer," Journal of Hydronautics, Vol. 10, No. 4, pp. 135-139, October 1976.

Lumley, J. L., "Drag Reduction in Turbu[illegible] Flow by Polymer Additives," Journal of Polymer Science, Macromolecular Reviews, Vol. 7, pp. 283-290, 1973.

Lumley, J. L., "Drag Reduction in Two Phase and Polymer Flows," Phys. of Fluids, Supplement, V20, N10, pp. 564-571, October 1977.

Morkovin, M. V., "On Eddy Diffusivity, Quasisimilarity and Chemical Reactions in Turbulent Boundary Layers," Int. J. Heat Mass Transfer, V8, pp. 129-145, 1965.

Parker, C. A., Photoluminescence of Solutions, Elsever, New York, 1968.

Poreh, M. and Cermak, J. E., "Study of Diffusion from a Line Source in a Turbulent Boundary Layer," Int. Journal of Heat and Mass Transfer, Vol. 7, pp. 1083-1095, 1964.

Pringsheim, P., Fluorescence and Phosphorescence, Interscience Publishers, Inc., p. 348, 1949.

Tennekes, H., and Lumley, J.L. A First Course in Turbulence, MIT Press, Cambridge, Massachusetts and London England, 1972.

Tiederman, W. G., Walker, D. T., and Bustetter, D. C., "Injection of Drag Reducing Additives into Turbulent Water Flows, Mixing Experiments and Newtonian Burst Frequency," Report PME-FM-87-1, Purdue University, 1987.

Toms, B. A., "Some Observations on the Flow of Linear Polymer Solutions through Straight Tubes at Large Reynolds Numbers," Proceedings 1st Int. Reol Congress, North Holland Publishing Co., 11, pt. 2, pp. 135-142, 1949.

Vdovin, A.V. and Smol'yakov, A.V., "Diffusion of Polymer Solutions in a Turbulent Boundary Layer," Zhurnal Prikladnoi Mekhaniki i Tekhnicheskoi Fiziki, No. 2, pp. 66-73, March-April 1978.

Vdovin, A.V. and Smol'yakov, A.V., "Turbulent Diffusion of Polymers in a Boundary Layer," Zhurnal Prikladnoi Mekhaniki i Tekhnicheskoi Fiziki, No. 4, pp. 98-104, July-August 1981.

Walker, D. A., "A Fluorescence Technique of Measurements of Concentration in Mixing Liquids," Journal of Physics E: Science Instru., Vol. 20, pp. 217-224, 1987.

Walker D. A. and Tiederman, W. G., "Injection of Drag Reducing Additives into Turbulent Water Flows - Concentration Results from Time Resolved Measurements," Report PME-FM-88-1, Purdue University, 1988.

Ware, W. R. and Baldwin, B. A., "Absorption Intensity and Fluorescence Lifetimes of Molecules," Journal of Chemical Physics, V40, pp. 1703-1705, 1964.

Wetzel, J. M. and Ripken, J. F., "Shear and Diffusion in a Large Boundary Layer Injected with Polymer Solution," Project Report No. 114, St. Anthony Falls Hydraulic Laboratory, University of Minnesota, 1970.

White, A. and Hemmings, J., Drag Reduction by Additives - Review and Bibliography, BHRA Fluid Engineering, Editor: J. Hemmings, Cranfield, England, 1976.

White, F.M. Viscous Fluid Flow, McGraw-Hill, New York, 1974.

Wick, R. A., "Quantum Limited Imaging Using Microchannel Plate Technology," Applied Optics, Vol. 26, No. 16, pp. 3210-3218, August 1987.

Wu, J. and Tulin, M. P., "Drag Reduction by Ejecting Additive Solutions into Pure Water Boundary Layers," Transaction of the ASME, Journal of Basic Engineering, pp. 749-756, December 1972.

APPENDIX

PROPERTIES OF FLUORESCEIN DISODIUM SALT

Fluorescence is a process in which a molecule absorbs a photon and is excited from its ground state into a singlet state. Upon returning to its ground state from the lowest vibrational level in the singlet state the molecule fluoresces. Since the lowest vibrational level in the singlet state is lower in energy than the initial excited state, the wavelength of the fluorescent light is longer than the absorbed wavelength.

The fluorescent dye, fluorescein disodium salt ($C_{20}H_{10}Na_2O_5x2H_2O$, MW 412.3), was chosen for use in the current study because it is highly soluble in water, has a high quantum yield, and a convenient absorption and emission wavelength. The absorption peak of fluorescein dye is 488nm which is identical to the radiation wavelength available with argon ion lasers. The fluorescence emission peak is 515nm which is conveniently close to the sensitivity peak of the photodiode array. Fluorescein fluoresces with a time constant of 5 nanoseconds [see Ware and Baldwin (1964)] and the radiation is randomly polarized and emitted uniformly in all directions.

While fluorescein is clearly a convenient dye to use for performing the concentration profile measurements there are several potential sources of error associated with its use which must be

considered. Fluorescein has a slight temperature dependence and an extreme pH dependence in the range from 4 to 7.5, Walker (1987). In the present study, the changes in tunnel water temperature and calibration flow cell fluid temperature are insignificant. The pH of the tunnel water was 7.4 and polymer solutions have pH values as high as 8.2. However, this range of pH can change the signal strength by only 5%.

Perhaps the most serious potential sources of error are, as discussed in section 4.2 Calibration, that the fluorescence intensity (i.e., the quantum yield) of fluorescein is dependent on the particular solvent used and that the fluorescence intensity of solutions containing fluorescein was observed to diminish with time. For a given laser beam intensity and dye concentration, solutions of polymer and fluorescein always had significantly higher fluorescence intensities than solutions of water and fluorescein. However, dilution experiments using tunnel water to dilute dyed polyox and dyed water solutions always resulted in a linear variation of fluorescence with concentration through the lowest concentration level measured. It appears that the polyox, even at very low concentrations, inhibits the reaction of the fluorescein with dissolved substances in the water and effectively maintains a quantum yield independent of polyox concentration. This is supported by the fact that the fluorescence decay of solutions of polyox and fluorescein is appreciably slower than with

solutions of water and fluorescein. Throughout the range of polyox concentrations examined, the rate at which the fluorescence decayed was the same. However, for both solutions of polymer and fluorescein and water and fluorescein the fluorescence decay rate decreased with time. These potential sources of error are the reasons why the calibrations are performed with the solutions which are to be ejected through the slot and why the use of aged solutions was adopted.

Another less serious potential source of error is photobleaching. Fluorescent dyes continuously exposed to excitation radiation undergo a photobleaching reaction to a non-fluorescing state. The fraction of photobleached molecules per photon absorbed is the bleaching efficiency and is small. Ippen (1971), et al, has determined the bleaching efficiency to be $Q_b = 4 \times 10^{-6}$ for fluorescein exposed to light at a 514.5nm wavelength. As discussed by Koochesfahani (1984), the number of active (absorbing) dye molecules η, as a function of time, is given by

$$\eta = \eta_0 \exp(-t/\tau_b)$$

where η_0 is the number of dye molecules at $t = 0$ and $1/\tau_b = Q_0 \Phi \sigma$ where

Φ= the laser photon flux in photons/cm^2/s

σ= the dye molecular cross section

The molecular cross section is determined from the extinction coefficient, ϵ, where $\sigma = (2300\epsilon)/N_{AV}$ and N_{AV} is Avogadros number

[see Parker (1968)]. The extinction coefficient is a measure of how rapidly a laser beam is attenuated by the presence of dye. ϵ is a function of the particular dye used and of the excitation wavelength. Using Walker's value of 8.72×10^4/(cm x mole/liter) for the extinction coefficient the time constant, τ_b, is 0.06 seconds for the present system. The transit time of a fluid element through the laser beam is considerably less than this at any resolvable distance above the wall in the present TBL flows.

An additional potential source of error is thermal blooming of the dye solution. Thermal blooming occurs when the dye solution is heated by the laser beam causing local index of refraction gradients. This causes the laser beam to diverge rapidly resulting in a marked decrease in the fluorescence intensity. Like photobleaching, problems with thermal blooming can be avoided by convecting the dyed fluid through the laser beam. Problems with photobleaching and thermal blooming can be quite severe for nonflowing systems.